

Disclosing connections between black holes and naked singularities: Horizon remnants, Killing throats and bottlenecks

Daniela Pugliese and Hernando Quevedo*

*Institute of Physics and Research Centre of Theoretical Physics and Astrophysics,
Faculty of Philosophy & Science, Silesian University in Opava,
Bezručovo náměstí 13, CZ-74601 Opava, Czech Republic*

Dipartimento di Fisica, Università di Roma "La Sapienza", I-00185 Roma, Italy

Instituto de Ciencias Nucleares, Universidad Nacional Autónoma de México, AP 70543, México, DF 04510, Mexico

Department of Theoretical and Nuclear Physics, Kazakh National University, Almaty 050040, Kazakhstan

(Dated: March 9, 2021)

We study the properties of black holes and naked singularities by considering stationary observers and light surfaces in Kerr spacetimes. We reconsider the notion of Killing horizons from a special perspective by exploring the entire family of Kerr metrics. To this end, we introduce the concepts of extended plane, Killing throats and bottlenecks for weak (slowly spinning) naked singularities. Killing bottlenecks (or horizon remnants in analogy with the corresponding definition of throats in black holes) are restrictions of the Killing throats appearing in special classes of slowly spinning naked singularities. Killing bottlenecks appear in association with the concept of pre-horizon regime introduced in [1, 2]. In the extended plane of the Kerr spacetime, we introduce particular sets, *metric bundles*, of metric tensors which allow us to reinterpret the concept of horizon and to find connections between black holes and naked singularities throughout the horizons. To evaluate the effects of frame-dragging on the formation and structure of Killing bottlenecks and horizons in the extended plane, we consider also the Kerr-Newman and the Reissner–Norström spacetimes. We argue that these results might be significant for the comprehension of processes that lead to the formation and eventually destruction of Killing horizons.

I. INTRODUCTION

One of the most important exact solutions of Einstein vacuum field equations is the Kerr metric, which in Boyer-Lindquist (BL) coordinates can be expressed as

$$ds^2 = -\frac{\Delta - a^2 \sin^2 \theta}{\rho^2} dt^2 + \frac{\rho^2}{\Delta} dr^2 + \rho^2 d\theta^2 + \frac{\sin^2 \theta \left((a^2 + r^2)^2 - a^2 \Delta \sin^2 \theta \right)}{\rho^2} d\phi^2 - 2 \frac{aM \sin^2(\theta) (a^2 - \Delta + r^2)}{\rho^2} d\phi dt, \quad (1)$$

$$\Delta \equiv r^2 - 2Mr + a^2, \quad \text{and} \quad \rho^2 \equiv r^2 + a^2 \cos^2 \theta. \quad (2)$$

It describes an axisymmetric, stationary, asymptotically flat spacetime. The parameter $M \geq 0$ is interpreted as the mass of the gravitational source, while the rotation parameter $a \equiv J/M$ (*spin*) is the *specific* angular momentum, and J is the *total* angular momentum of the source. The spherically symmetric (static) Schwarzschild solution corresponds to the limiting case with $a = 0$. If the spin-mass ratio is within the range $a/M \in]0, 1[$, the spacetime corresponds to a Kerr black hole (**BH**). The extreme black hole case is defined by the relation $a = M$, whereas a super-spinner Kerr compact object or a naked singularity (**NS**) geometry occurs when $a/M > 1$.

The Kerr metric tensor (1) has several remarkably properties.

(i) The metric (1) is invariant under the application of any two different transformations of the form $\mathcal{P}_{\mathbf{Q}} : \mathbf{Q} \rightarrow -\mathbf{Q}$, where \mathbf{Q} is one of the coordinates (t, ϕ) or the metric parameter a : a single transformation leads to a spacetime with an opposite rotation with respect to the unchanged metric.

(ii) The Kerr solution is stationary and axisymmetric due to the presence of the Killing fields $\xi_t = \partial_t$ and $\xi_\phi = \partial_\phi$, respectively.

*Electronic address: d.pugliese.physics@gmail.com

An observer moving with uniform angular velocity along the curves $r = \text{constant}$ and $\theta = \text{constant}$ will see a spacetime which does not change at all (therefore, the covariant components p_ϕ and p_t of the particle four-momentum are conserved along the circular geodesics).¹

(iii) As the metric is invariant under reflections with respect to the equatorial hyperplane $\theta = \pi/2$, equatorial trajectories are confined in the equatorial geodesic plane.

For black hole and extreme black hole spacetimes, the radii

$$r_\pm \equiv M \pm \sqrt{M^2 - a^2}, \quad (3)$$

solutions of $g^{rr} = 0$, are the radii of the outer and inner Killing horizons, whereas

$$r_\epsilon^\pm \equiv M \pm \sqrt{M^2 - a^2 \cos^2 \theta}, \quad (4)$$

solutions of $g_{tt} = 0$, are the outer and inner *ergosurfaces*, respectively, with $r_\epsilon^- \leq r_- \leq r_+ \leq r_\epsilon^+$. In an extreme **BH** geometry, the horizons coincide, $r_- = r_+ = M$, and the relation $r_\epsilon^\pm = r_\pm$ is valid on the rotational axis (i.e., when $\cos^2 \theta = 1$). In the Kerr **BH** spacetime, the Killing vector representing time translations at infinity, ∂_t , becomes null on the outer ergosurface, r_ϵ^+ , which is, however, a *timelike* surface. On the contrary, a Killing horizon is a lightlike hypersurface (generated by the flow of a Killing vector) on which the norm of a Killing vector vanishes. That is, the Kerr horizons are *null* surfaces, \mathcal{S}_0 , whose *null* generators coincide with the orbits of an one-parameter group of isometries, i.e., in general there exists a Killing field \mathcal{L} , which is normal to \mathcal{S}_0 .

Some additional properties of the Kerr spacetime include:

(iv) In the limiting case of the Schwarzschild spacetime ($a = 0$), $r = 2M$ is the Killing horizon with respect to the Killing vector ∂_t . In general, in the special case of static (and spherically symmetric) **BH** spacetimes, the event, apparent, and Killing horizons with respect to the Killing field ξ_t coincide.

(v) The event horizons of a spinning **BH** are Killing horizons with respect to the Killing field $\mathcal{L}_H = \partial_t + \omega_H \partial_\phi$, where ω_H is the angular velocity of the horizon.

In this work, we extensively discuss the properties of the Killing vector $\mathcal{L} = \partial_t + \omega \partial_\phi$ in the case of **NS** geometries. In **BH** spacetimes, this vector plays a crucial role in defining thermodynamic variables. As we will see below, the velocity ω (and its limit ω_H) and the vector \mathcal{L} (and its limit \mathcal{L}_H) are important for defining horizons and establishing relations between black holes and extreme black holes. In fact, it can be shown that: (a) In the context of the rigidity theorem, ω_H represents the **BH** rigid rotation. Stated differently, the (strong) rigidity theorem connects the event horizon with a Killing horizon. In fact, under certain conditions, the event horizon of a stationary asymptotically flat solution (with matter satisfying suitable hyperbolic equations) is a Killing horizon. (b) The **BH** event horizon of this stationary solution is moreover a Killing horizon with constant surface gravity (zeroth **BH** law—the surface gravity is constant on the horizon of stationary black holes) [3, 4]. (c) Finally, the surface area of the **BH** event horizon is non-decreasing in time, which is the content of the second **BH** law (the laws state also the impossibility to achieve by a physical process a **BH** state with surface gravity $\kappa = 0$.)

We note here that the surface gravity of a **BH** may be defined as the rate at which the norm of the Killing vector vanishes from the outside. (The surface gravity is related to the acceleration of a particle corotating with the **BH** at the horizon and it can be written as $(\mathcal{S}G_{Kerr} = (r_+ - r_-)/2(r_+^2 + a^2))$. It is, therefore, a conformal invariant of the metric).

Possibly, we could isolate the contribution of the rotation in the expression of the surface gravity by comparing it with the static (and spherically symmetric) metric of Schwarzschild. In fact, the Kerr **BH** surface gravity can be written as the combination $\kappa = \kappa_s - \gamma_a$, where $\kappa_s \equiv 1/4M$ is the Schwarzschild surface gravity, while $\gamma_a = M\omega_H^2$ is the contribution due to the additional component of the **BH** intrinsic spin; ω_H is, therefore, the angular velocity (in units of $1/M$) on the event horizon.

These laws, which depend also on the horizon angular velocity, impose important constraints on any physical process in the **BH** spacetime, but they also allow to distinguish the static solution, $a = 0$, from the Kerr **BH** solution. The first law of **BH** thermodynamics, applied to a Kerr **BH** spacetime, actually relates the variation of the **BH** mass, horizon area and angular momentum, including the surface gravity and angular velocity on the horizon, i.e., $\delta M = (1/8\pi)\kappa\delta A + \omega_H\delta J$. In here, the term dependent on the **BH** angular velocity represents the “work term” of the first law, while the fact that the surface gravity is constant on the **BH** horizon, together with

¹ We use geometrical units with $c = 1 = G$ and the signature $(-, +, +, +)$, Greek indices run in $\{0, 1, 2, 3\}$. The four-velocity satisfies the condition $u^\alpha u_\alpha = -1$. The radius r has units of mass $[M]$, and the angular momentum units of $[M]^2$, the velocities $[u^t] = [u^r] = 1$ and $[u^\phi] = [u^\theta] = [M]^{-1}$ with $[u^\phi/u^t] = [M]^{-1}$ and $[u_\phi/u_t] = [M]$. For the sake of convenience, we consider a dimensionless energy and an angular momentum per unit of mass $[L]/[M] = [M]$.

other considerations, allows us to associate it with the concept of temperature. This aspect tends to emphasize the difference (also topological) between Kerr's **BH** and its extreme solution: in the extreme case, where $(r_{\pm} = M)$, it is easy to see that the surface gravity is zero and, considering the association with the temperature, there is $T_H = 0$, with consequences also with respect to the stability against Hawking radiation. Nevertheless, the entropy (or **BH** area) of an extremal **BH** is not null[3–10]. (An analogue implication of the third law it is said that a non-extremal **BH** cannot reach an extremal case in a finite number of steps.)

We investigate the properties of Kerr **BHs** and **NSs** from the point of view of stationary observers. In particular, we explore the characteristics of light surfaces, which correspond to the limiting frequencies of stationary observers. From the analysis of these orbital frequencies (and associated orbits), we introduce the concept of Killing throats, arising in **NS** spacetimes as the “opening” and disappearance of Killing horizons. More precisely, the Killing throat is a region bounded by a particular set of curves that we identify with the frequency of a stationary observer, which depends on the radial distance and the spin parameter a of the source. We define a Killing bottleneck as a particular case of a Killing throat that appears in weak naked singularities (**WNS**). Thus, bottlenecks can be interpreted as throats “restrictions” that characterize **WNS**. The concept of strong and weak **NSs** depends on the value of the spin parameter and has been explored in several works [11–18]. However, in general, they are also differently defined as strong curvature singularities, for example, in [19]. Regarding various **NSs** properties and characteristics of the gravitational collapse, possible formation and stability of naked singularities as well as other analysis concerning observational phenomena related to possible **NSs** existence, we refer also to [20–33, 37–41]. In this work, **WNSs** are characterized by spin-mass ratios close to the value of the extreme **BH**. To explore these **NS** effects and to compare **BHs** with **NSs**, it is convenient to introduce the concept of “metric bundles” and “extended planes”. A metric bundle is a curve on the extended plane, i.e., a family of spacetimes defined by one characteristic photon orbital frequency ω and characterized by a particular relation between the metrics parameters. This turns out to establish a relation between **BHs** and **NSs** in the extended plane. All the metric bundles are tangent to the horizon curve in the extended plane. Then, the horizon curve emerges as the envelope surface of the set of metric bundles. As a consequence, **WNSs** turn out to be related to a part of the inner horizon, whereas strong naked singularities (**SNSs**) with $a > 2M$ are related to the outer horizon.

This work is organized as follows. In Sec. (II), we study the main definitions and properties of stationary observers and light surfaces in **BH** and **NS** Kerr geometries. Killing throats and bottlenecks are the focus of Sec. (III). In Sec. (IV), we introduce the concept of metric bundles and discuss the resulting connections between **BHs** and **NSs**. These results are generalized to include the cases of the Kerr-Newman and Reissner-Nordström spacetimes in Sec.(V). Concluding remarks and future perspectives follow in Sec. (VI). This article closes with two Appendices. The off-equatorial case in the Kerr and Kerr-Newman geometries is considered in Appendix A. In Appendix B, we study the areas of the horizons and regions of the extended plane delimited by different metric bundles. Throughout this work, we introduce a considerable number of symbols and notations which are necessary to explain all the details of the results we will obtain. For clarity, we list in Table I the main symbols and their definitions.

II. STATIONARY OBSERVERS AND LIGHT SURFACES

Stationary observers have a tangent vector which is a spacetime Killing vector; their four-velocity is, therefore, a linear combination of the two Killing vectors ξ_{ϕ} and ξ_t as:

$$d\phi/dt = u^{\phi}/u^t \equiv \omega, \quad \text{or} \quad u^{\alpha} = \gamma(\xi_t^{\alpha} + \omega\xi_{\phi}^{\alpha}), \quad (5)$$

$$\text{with} \quad \gamma^{-2} \equiv -\varepsilon(\omega^2 g_{\phi\phi} + 2\omega g_{t\phi} + g_{tt}), \quad (6)$$

where ω (a dimensionless quantity) is the (uniform) *angular velocity*, while γ is a normalization factor ($g_{\alpha\beta}u^{\alpha}u^{\beta} = -\varepsilon$).

Because of the symmetries, the coordinates r and θ of a stationary observer are constants along its worldline, consequently a stationary observer does not see the spacetime changing along its trajectory. Timelike stationary observers have angular velocity bounded in the range

$$\omega \in]\omega_-, \omega_+[\quad \text{where} \quad \omega_{\pm} \equiv \omega_Z \pm \sqrt{\omega_Z^2 - \wp^2}, \quad (7)$$

$$\wp^2 \equiv \frac{g_{tt}}{g_{\phi\phi}} = \frac{g^{\phi\phi}}{g^{tt}}, \quad \wp^{-2} \equiv \frac{g^{tt}}{g^{\phi\phi}} = \frac{g_{\phi\phi}}{g_{tt}}, \quad \omega_Z \equiv -\frac{g_{\phi t}}{g_{\phi\phi}},$$

TABLE I: Lookup table with the main symbols and relevant notations used throughout the article.

ω_{\pm}	limiting frequencies for stationary observers: Eqs.(7)-(8)
$\omega_0 = M/a$	limiting frequency ω_{\pm} at the singularity and frequency of the metric bundle: Eq. (9)-Sec. (IV)
\mathcal{L}_{\pm}	null Killing vector (generators of Killing event horizons): Eq. (10)
r_s^{\pm}	light surfaces radii: Eq. (11)
ω_H^{\pm}	frequencies at the horizons r_{\pm} : Eq. (12)
r_{\pm}^{\mp}	photon orbits with frequencies ω_H^{\pm} at the horizons: Eq. (13)–Fig. 1
g_{ω}^{\pm}	metric bundles in the extended plane π_a : Sec. (IV)
$a_{\omega}^{\pm}(r, \omega; M)$	g_{ω}^{\pm} in terms of the bundle frequency ω : Eq. (15)
a_{\pm}	horizon curve in the extended plane: Fig. (8)
$r_{\partial}^{\pm}(\omega)$	closing radii of the metric bundle in π_a^+ ($=\pi_a$ for $a > 0$): Eq. (16)
a_g	spin of metric bundle tangent to the horizons in π_a^+ : Eq. (17)– Fig. (13)
a_p	bundle origin, i.e., $a_g(a_0) = a_g(a'_0)$ with $a'_0 = a_p \equiv 4M^2/a_0$: Figs. 14, 15, 16; Tables III and II
horizons relations I	$\omega_0^{-1} \equiv a_0^{\pm}/M = \frac{2r_{\pm}(a_g)}{a_g} \equiv \omega_H^{-1}(a_g)$, $\omega_H^+(r_g, a_g) = \omega_0 = Ma_0^{-1}$, $\omega_H^-(r'_g, a_g) = \omega'_0 = M/a'_0$ $r'_g \in r_-$ ($r_+ = r_g$, $r_- = r'_g$): Fig. (13)
horizons relations II	$\omega'_0 = \frac{1}{4\omega_0}$, $\omega_H^+\omega_H^- = \frac{1}{4}$, $(a_0^+(a_g)a_0^-(a_g) = 4M^2)$, $a_0^{\pm}/M = \frac{2r_{\pm}(a_g)}{a_g}$ where $a = a_0$ and $a = a_p$: Fig. 14
SNS	(= SNS ⁺ \cup SNS ⁻) strong naked singularities $a_0 > 2M$, SNS ⁺ for $a_0 > 4M$ SNS ⁻ for $a_0 \in [2M, 4M[$: Fig. (13)
WNS	weak naked singularities $a_0 \in]M, 2M[$: Fig. (13)
BH = BH ⁺ \cup BH ⁻	BH ⁺ for $a \in [a_g^1, M]$, $a_g^1 = 3/4M$ and BH ⁻ for $a \in [0, a_{g1}]$: Fig. (13)
<i>Left region</i> Fig. (13)	$a_0 \in [0, 2M]$
<i>Right region</i> Fig. (13)	$a_0 > 2M$
<i>up-sector</i> Fig. (13)	$a_g > a_g^1$
<i>down-sector</i> Fig. (13)	$a_g < a_g^1$
ϖ_{\pm}	second frequency of a metric bundle: Eq. (22)
$a_{\omega}^{(b)}(\omega_H^b)$	metric bundles parameterized for the tangent point a_g : Eq. (23)
$a_{tangent}(r)$	tangent curve to the horizon in terms of r_g : Eq. (24)
$(r_g^{real}, r_g^{\vee}, r_g^{\mp})$	solution of the tangency condition $a_g = a_{\pm}$: Eq. (25), Fig. (17)
$(Q_{\omega}^{\pm})^2$	metric bundles in terms of the charge Q : Eq. (35)

($\varepsilon = +1$)². Zero Angular Momentum Observers (ZAMOs) are defined by the condition $\mathcal{L}_{\mathcal{Z}AM\mathcal{O}} = 0$ and have angular velocities ω_Z , which depend on the spin. A ZAMO, well defined in the ergoregion, corotates with the **BH**. ZAMOs have interesting properties in the case of slowly spinning naked singularities and certainly offer a particularly appropriate and convenient description of the spacetime in the ergoregion –see for example [16, 18] and [42–54]. Static observers are defined by the limiting condition $\omega = 0$ and cannot exist in the ergoregion. The particular frequencies ω_{\pm} provide an alternative definition of the horizons. Since the horizons are null surfaces, it should hold that $\omega_+ = \omega_-$, which is the limiting angular velocity for physical observers corresponding in fact to orbital photon frequencies. The quantity in parenthesis in the r.h.s. of Eq. (6) becomes null for photon-like particles and the rotational frequencies ω_{\pm} , as in Eq. (7). On the equatorial plane, the limiting orbital frequencies are

$$\omega_{\pm} \equiv \frac{2aM^2 \pm M\sqrt{r^2\Delta}}{r^3 + a^2(2M+r)}, \quad \omega_{\pm}(r_+) = \omega_Z(r_+) = \omega_H \equiv \frac{a}{2r_+} \equiv \frac{M}{2\omega_0 r_+}. \quad (8)$$

The following limits are valid

$$\lim_{r \rightarrow \infty} \omega_{\pm} = 0, \quad \lim_{a \rightarrow \infty} \omega_{\pm} = 0, \quad \lim_{r \rightarrow 0} \omega_{\pm} = \omega_0 \equiv \frac{M}{a}. \quad (9)$$

The limit $a \rightarrow \infty$ is used to formally explore the behavior in the strong **NS** singularity regime, for a given constant value of M , and more generally in the limit $a \gg M$. As already mentioned in Sec. (I), the Killing vector

$$\mathcal{L}_{\pm} \equiv \xi_t + \omega_{\pm} \xi_{\phi} \quad (10)$$

can be read as generator of null curves ($g_{\alpha\beta} \mathcal{L}_{\pm}^{\alpha} \mathcal{L}_{\pm}^{\beta} = 0$) as the Killing vectors \mathcal{L}_{\pm} , null at $r = r_+$, are also generators of Killing event horizons.

² This equation corrects a typo in Eq. (8) of Ref. [18]

The expression (7) for the frequency of a stationary observer can be considered as an equation for the radii of the light surfaces r_s^\pm . The solutions are then given as functions of the frequency ω and can be written as [18]

$$\frac{r_s^-}{M} \equiv \frac{2\beta_1 \sin\left(\frac{1}{3} \arcsin \beta_0\right)}{\sqrt{3}}, \quad \frac{r_s^+}{M} \equiv \frac{2\beta_1 \cos\left(\frac{1}{3} \arccos(-\beta_0)\right)}{\sqrt{3}} \quad (11)$$

where $\beta_1 \equiv \sqrt{\frac{1}{\omega^2} - \frac{1}{\omega_0^2}}$, $\beta_0 \equiv \frac{3\sqrt{3}\beta_1\omega^2}{\left(\frac{\omega}{\omega_0} + 1\right)^2}$.

III. KILLING THROATS AND BOTTLENECKS

The concept of Killing throats emerges through the analysis of the radii $r_s^\pm(\omega, a)$ (the frequencies $\omega_\pm(r, a)$) with respect to the orbital frequency ω (the radius r) of light-like particles – see Figs. 2 and 3. A Killing throat in **NS** geometries is a connected region in the $r-\omega$ plane, which is bounded by $r_s^\pm(\omega, a)$ or equivalently $\omega_\pm(r, a)$, and contains all the stationary observers allowed within the limiting frequencies $]\omega_-, \omega_+[$. Conversely, a **BH** Killing throat is either a disconnected region in the Kerr spacetime (in a sense similar to the concept of a path-connected space) or a region bounded by non-regular surfaces in the extreme Kerr **BH** spacetime. A *Killing bottleneck in a NS spacetime is a narrowing of the Killing throat which appears only for specific naked singularities and involves a narrow range of frequencies and orbits–Figs (1)*. The limiting case of a Killing bottleneck occurs in the extreme Kerr spacetime, as seen in the BL frame, where the narrowing actually closes³ at the **BH** horizon $r = M$.

More generally, the Kerr horizons determine the following frequencies:

$$\omega_H^\pm \equiv \frac{a}{2r_\pm} \equiv \omega_\pm(r_\pm) \quad \text{with} \quad \omega_H^+ < \omega_H^- \quad \text{for} \quad a > 0 \quad \text{and} \quad \omega_H^\pm = \frac{1}{2} \quad \text{for} \quad a = M. \quad (12)$$

It should be noted then that while the horizons radii are functions of the metric parameters only, meaning that there is only one frequency, ω_H^\pm , on the horizons r_\pm , respectively, the Killing bottlenecks depend on both frequency and radius, corresponding to the fact that the throat never closes, but in the limit of the extreme Kerr spacetime.

Considering again the horizons frequencies ω_H^\pm , we introduce the radii r_\mp^\mp representing the set of photon orbits with frequencies ω_H^\pm at the **BH** horizons

$$r_-^- : \quad \omega_-(r_-^-) = \omega_-(r_-) = \omega_H^- \quad \text{where} \quad r_-^- = \frac{1}{2} \left(\sqrt{\frac{32M^3r_-}{a^2} - a^2 + 6M\sqrt{M^2 - a^2} - 22M^2 - r_-} \right) \quad (13)$$

$$r_+^+ : \quad \omega_+(r_+^+) = \omega_+(r_+) = \omega_H^+, \quad \text{where} \quad r_+^+ = \frac{1}{2} \left(\sqrt{\frac{32M^3r_+}{a^2} - a^2 - 6M\sqrt{M^2 - a^2} - 22M^2 - r_+} \right), \quad (14)$$

with $r_-^- < r_- < r_+ < r_+^+$ – see Fig. 1. In Sec. IV, this property is displayed in a different context, showing a close connection between **BHs** and **NSs**. Moreover, the Killing horizons, r_\pm , are defined as the tangent (envelope surfaces) of the curves defined by the conditions $\omega_\pm(r, a) = \text{constant}$. The existence of $r_+^+ > r_+$ implies that an observer could eventually measure the frequency of the outer horizon ω_H^+ on the equatorial plane, while *no information* can be obtained from r_-^- for the inner horizon frequency ω_H^- . In this sense, we may call this property as *inner horizon confinement*. This situation can be used to distinguish between slow rotating **BHs** and fast spinning **BHs** since the distance $(r_+^+ - r_+)$ decreases with the spin. The existence of these radii may be related to the bottleneck presence.

Figure 2 shows the formation of the Killing throat as the spin of the naked singularity varies. The emergence of the Killing bottleneck in terms of the frequency ($\omega - r$ plane) and of the radius ($r - \omega$ plane) is evident in the case of weak naked singularities, i.e., slow spinning singularities. We specify below the limiting spin values which define weak naked singularities. To evaluate the effects of the spacetime dragging on the formation of a Killing bottleneck, we investigate in Sec. (V) the Kerr-Newman geometry, the limiting static case of the Reissner Nordström geometry, and the off-equatorial case.

Three distinct phases are significant in the process of formation of bottlenecks:

³ Killing throats and bottlenecks, represented Figs (1) and (2), were grouped in [34] in structures named “whale diagrams”, considering the escape cones, particles motion and collisionals problems in the Kerr and Kerr-Newman spacetimes—see also [35, 36].

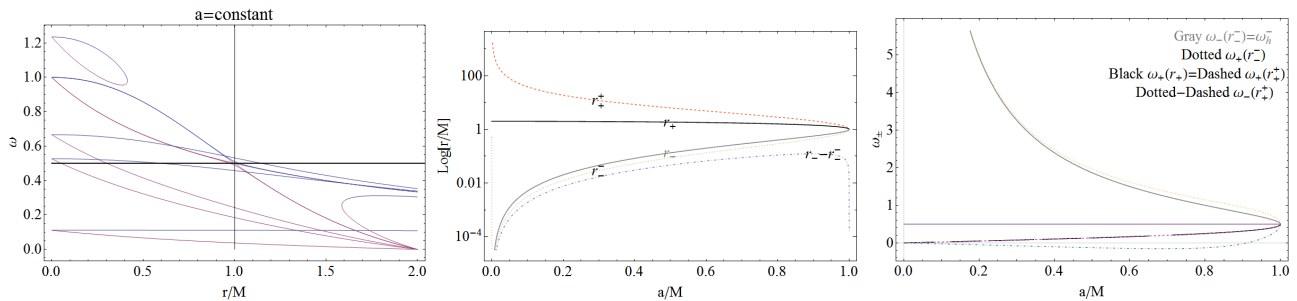


FIG. 1: Left panel: Frequencies ω_{\pm} for fixed values of the spin a/M for **BHs** and **NSs**. The coalescence of the Killing horizons r_{+} and r_{-} in the extreme black hole geometries and the emergence of a Killing throat and a Killing bottleneck in the **NS** geometries are clear –see also Figs (2,11,27,28), and Figs (26). Center panel: Killing horizons, r_{\pm} , and radii (r_{-}, r_{+}^{\pm}) as given in Eq. (13). Right panel: Frequencies ω_{\pm} in r_{\pm} and (r_{-}, r_{+}^{\pm}) as functions of a/M .

- (1) Coalescence of the Killing horizons, which occurs in the extreme Kerr **BH** solution;
- (2) Formation of the Killing throat and emergence of the bottleneck in weak **NSs**;
- (3) Disappearance of the Killing bottleneck in strong **NSs**.

The analysis carried out in Figs. 2 and 5 suggests that the Killing bottlenecks can be defined through the conditions $r_{III}^{\pm} : \partial_{\omega}^3 r_s^{\pm} = 0$ and $\omega_{III}^{\pm} : \partial_{\omega}^3 r_s^{\pm} = 0$. On the other hand, the radii $r_{II}^{\pm} : \partial_{\omega}^2 r_s^{\pm} = 0$ and, analogously, $\omega_{II}^{\pm} : \partial_r^2 \omega_{\pm} = 0$ characterize the curvatures of the curves ω_{\pm} and r_s^{\pm} .

Killing bottlenecks, identified in [18] as ripples in the $r-\omega$ plane (see Figs. 3 and 4), were interpreted in the **BL** frame as “remnants” of the disconnection between the Killing throat present in **BH**-geometries and the singular bottleneck of the extreme **BH**. The radii r_{III}^{\pm} and the frequencies ω_{III}^{\pm} , as shown in Fig. 5, define closed and limited surfaces. This implies that a Killing throat can always exist, but a Killing bottleneck appears only for certain frequencies and values of the dimensionless spin a/M . In fact, r_{III}^{\pm} is defined for **NSs** with spin $a \in]M, a_f]$, where $a_f = 1.840M$. On the other hand, r_{III}^{\pm} and ω_{III}^{\pm} are not closed and ω_{III}^{\pm} tends to the horizon frequency $\omega_H^{-} > \omega_H^{+}$ for very small spins. This means that the Killing bottleneck actually survives only for $a \in]M, a_{\bullet}]$, where $r_{III}^{-} = r_{III}^{+}$ at $a_{\bullet} = 1.668M < a_f$. However, the bottleneck frequencies satisfy the inequalities $\omega_{III}^{-} < \omega_H^{+} < \omega_H^{-} < \omega_{III}^{+}$. Increasing the spin a/M , at constant mass, a bending of the frequency ω_{-} appears⁴.

There are several notable radii associated with the frequencies ω_{\pm} and light surfaces r_s^{\pm} , which are related to the extremes and saddle points of the curves in the region Σ_c^{+} (see [18]). The function $\Delta\omega \equiv \Delta^{\pm}\omega = \omega_{+} \pm \omega_{-}$ is considered in Figs. 6 and 7. The radius r_{Δ} , solution of $\partial_r \Delta\omega = 0$, clearly shows the presence of closed surfaces for r_{III}^{\pm} and r_{II}^{\pm} , and provides a characterization of the Killing bottleneck. An analysis of ω_{\pm} and $\Delta\omega$ in Figs. 6 and 7 shows the emergence of horizons as the envelope surface in the plane $r-a$ of the limiting frequencies ω_{\pm} . This important aspect will be addressed in details in Sec. IV, revealing the role played by the Killing horizons in **BHs-NSs** connections.

IV. UNVEILING BHS–NSS CONNECTIONS

In this section, we explore the entire parameterized family of Kerr solutions with $a/M \geq 0$. To this end, we introduce the concept of extended plane π_a , where the entire collection of metrics of a parametrized family of solutions can be considered.

We may say that a quantity $\mathcal{Q}(a)$ in the plane π_a induces a $\mathcal{Q}-a$ realization of the extended plane, where a is a parameter that characterizes the entire family of solutions. For the case considered in this work, a is the dimensionless spin parameter. A special and simple example of an extended plane realization is given in Fig. 8, where we investigate constant frequency surfaces defining families of spacetime geometries that we call “metric-bundles”, g_{ω}^{\pm} , labeled by a frequency parameter $\omega = \text{constant}$. Such definitions are set from the properties of stationary observers and their limiting frequencies ω_{\pm} . In the extended plane, naked singularities and black holes can belong to the same metric

⁴ Note that the Killing bottleneck and Killing throat inherit some of the properties of the Killing vectors, particularly, regarding conformal transformations of the metric or vectors. Consider a Killing throat defined by two Killing vectors (ξ_i, ξ_j) . The linear combination $a_{\alpha}\xi^{\alpha}$ defines a Killing vector and we can define a Killing field up to a conformal transformation. In other words, $\mathcal{L} = \xi_t + a_{\phi}\xi_{\phi}$ identifies a Killing throat up to a conformal transformation. The simplest case is when one considers a conformal expanded (or contracted) spacetime where $\tilde{\xi}^2 \equiv \tilde{\mathbf{g}}(L, L) = \Xi^2 \mathbf{g}(L, L)$. This holds also for a conformal expanded Killing tensor $\tilde{\mathcal{L}} \equiv \Xi \mathcal{L}$.

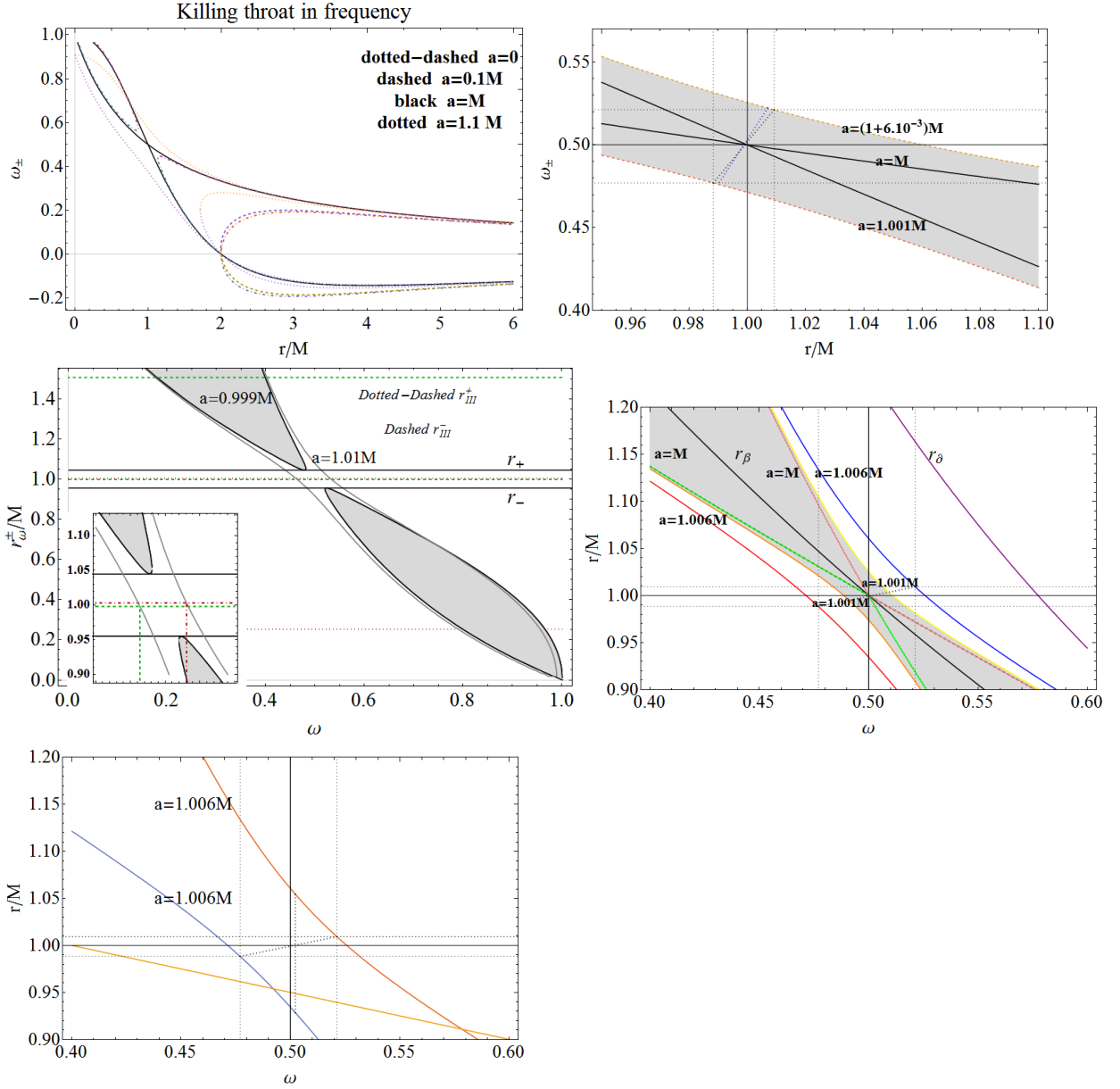


FIG. 2: Equatorial plane of the Kerr spacetime. Killing throat: zoom of the Killing bottleneck. Upper panels: The plane ω - r/M with plots of ω_{\pm} for different spins a/M . Left upper panel: Light surfaces for different **BHs** to **NSs**. As a/M changes for weak naked singularities, the narrowing of the light surfaces is shown explicitly. Right upper panel: Light surfaces in the bottleneck and the corresponding relevant radii. Bottom panels: The plane r/M - ω with plots of the radii of stationary observers r_s^{\pm} for different spins a/M . Center and right bottom panels: Zoom on the Killing bottleneck and relevant radii. The radii r_{III}^{\pm} (solutions of $\partial_r^3 \omega_{\pm} = 0$) are shown as functions of the spin a/M . The radii r_{β} and r_{δ} are defined in Eq. (16) and Eq. (B1), respectively.

bundle. In the extended plane of Fig. 8, **BHs** horizons r_{\pm} correspond to the spin-curve $a_{\pm}(r) \equiv \sqrt{r(r-2M)}$; we shall see that in such a plane the **BHs** horizons $a_{\pm}(r)$ define properties for *all* possible Kerr geometries, including **BHs** and **NSs**, that unveil an interesting connection between **BHs** and **NSs**.

Metric bundles g_{ω}^{\pm}

Here, we specify the idea of metric bundles for the Kerr family of solutions. Solving Eq. (8) for the spin a , we obtain the following two quantities

$$a_{\omega}^{\pm}(r, \omega; M) \equiv \frac{2M^2\omega \pm \sqrt{r^2\omega^2 [M^2 - r(r+2M)\omega^2]}}{(r+2M)\omega^2}, \quad (15)$$

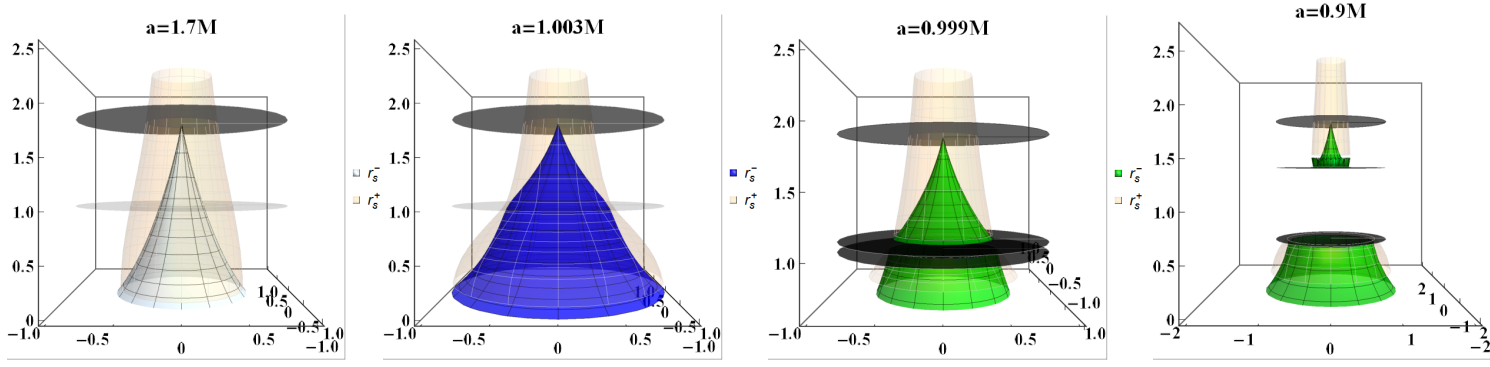


FIG. 3: Plots of the surfaces r_s^\pm (in units of mass) versus the frequency ω for different spin values a/M , including **BH** and **NS** geometries. The surfaces r_s^\pm are represented as revolution surfaces with height r_s^\pm (vertical axes) and radius ω (horizontal plane). Surfaces are generated by rotating the two-dimensional curves r_s^\pm around an axis (revolution of the function curves r_s^\pm around the “z” axis). Thus, $r = \text{constant}$ with respect to the frequency ω is represented by a circle. The disks in the plots are either $r = M$, $r = r_\pm$ (black) or $r = r_\epsilon^+ = 2M$.

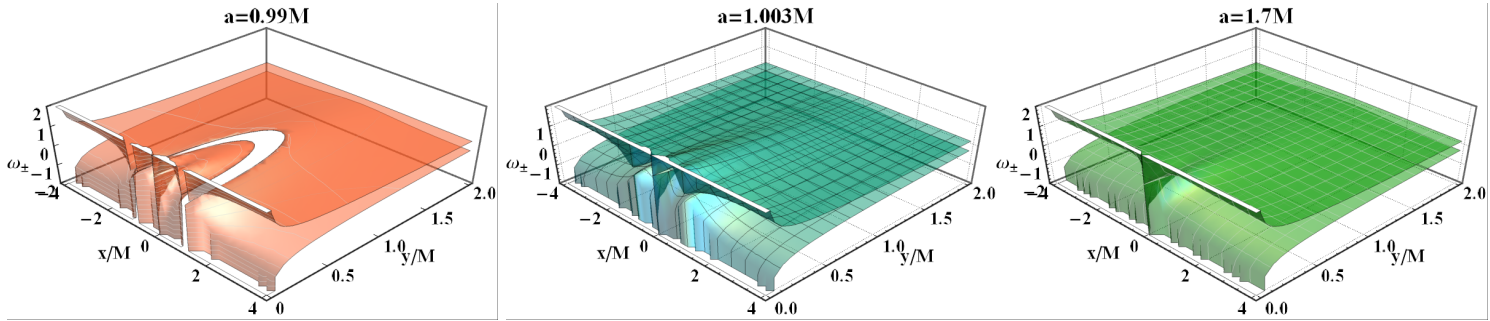


FIG. 4: Plots of the frequency surfaces $\omega_\pm(r, \theta)$ as functions of the radial distance r/M in Cartesian coordinates (x, y) for different spin values a , including **BHs** and **NSs**.

which are plotted in Figs 8 and 9 as functions of r/M , for different values of the frequency ω . Note that in the region $r > r_\epsilon^+$, negative orbital frequencies are possible because they are associated to the retrograde (counterrotating) motion with respect to the central object; this fact implies the possibility of negative values of a_ω^\pm for $\omega > 0$ —see Figs. 8. However, in this section, we restrict our analysis to the ergoregion Σ_ϵ^+ , where $a > 0$ and $\omega > 0$ —see Figs. 8 and 9. Each spacetime of the Kerr family is represented (restricted to the equatorial plane) in the extended plane of Fig. 8 by a constant surface $a_\omega^\pm/M = \text{constant}$ (horizontal lines in Fig. 8).

The metric bundles $g_\omega \equiv g_\omega^\pm$ are defined by the curves $a_\omega^\pm|_\omega$ of constant frequency ω in π_a —Fig. 8. Each $g_\omega = a_\omega^\pm|_\omega$ for a fixed frequency $\bar{\omega}$ is represented by closed and bounded curves which are continuous almost everywhere in π_a . Below, we will discuss extensively the properties of these curves.

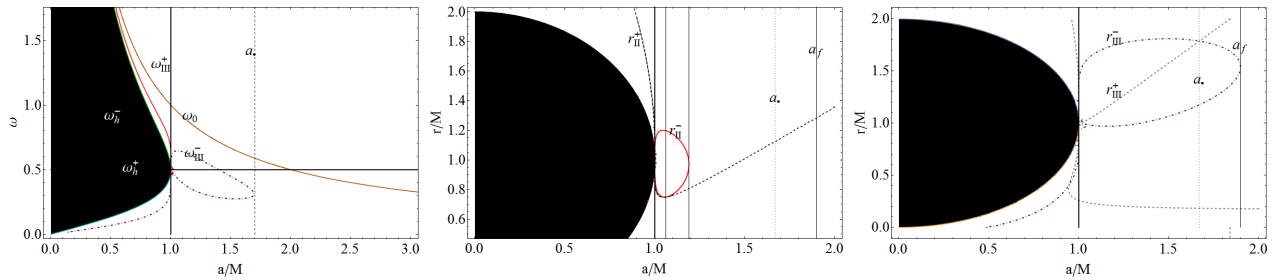


FIG. 5: Center-right panels. The radii r_{II}^\pm and r_{III}^\pm , solutions of $\partial_r^2 \omega_\pm = 0$ and $\partial_r^3 \omega_\pm = 0$, respectively, are shown as functions of the spin a/M . Black regions correspond to $r < r_\pm$. Left panel: The frequencies ω_{II}^\pm and ω_{III}^\pm , solutions of $\partial_\omega^2 r_s^\pm = 0$ and $\partial_\omega^3 r_s^\pm = 0$, respectively, are shown as functions of the spin a/M . Regions bounded by the horizons frequencies ω_H^\pm are black shaded.

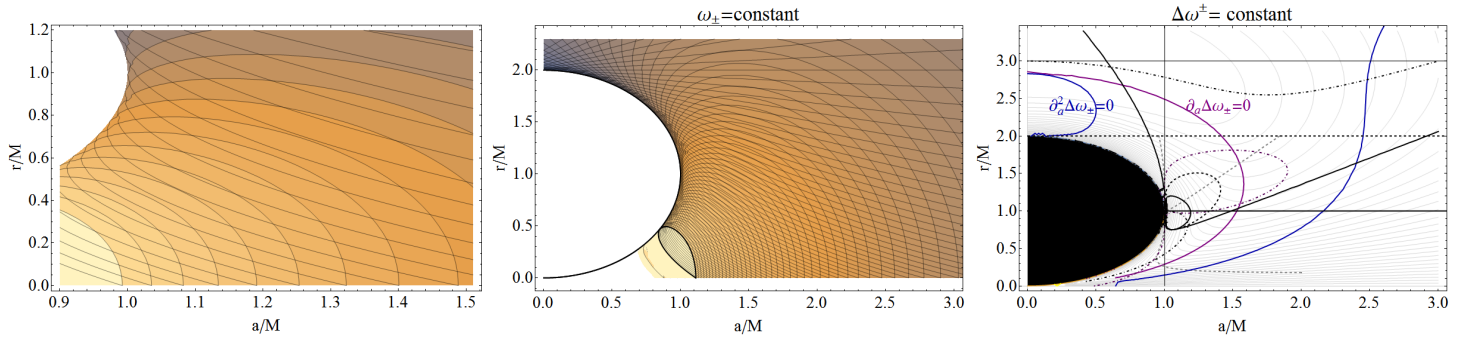


FIG. 6: Left and center panels: Curves $\omega_{\pm} = \text{constant}$ in different geometries with spacetime dimensionless spin a/M . Horizons are black thick lines. Right panel: Curves $\Delta^{-}\omega \equiv \omega^{+} - \omega^{-} = \text{constant}$ and notable radii—see Figs 5.

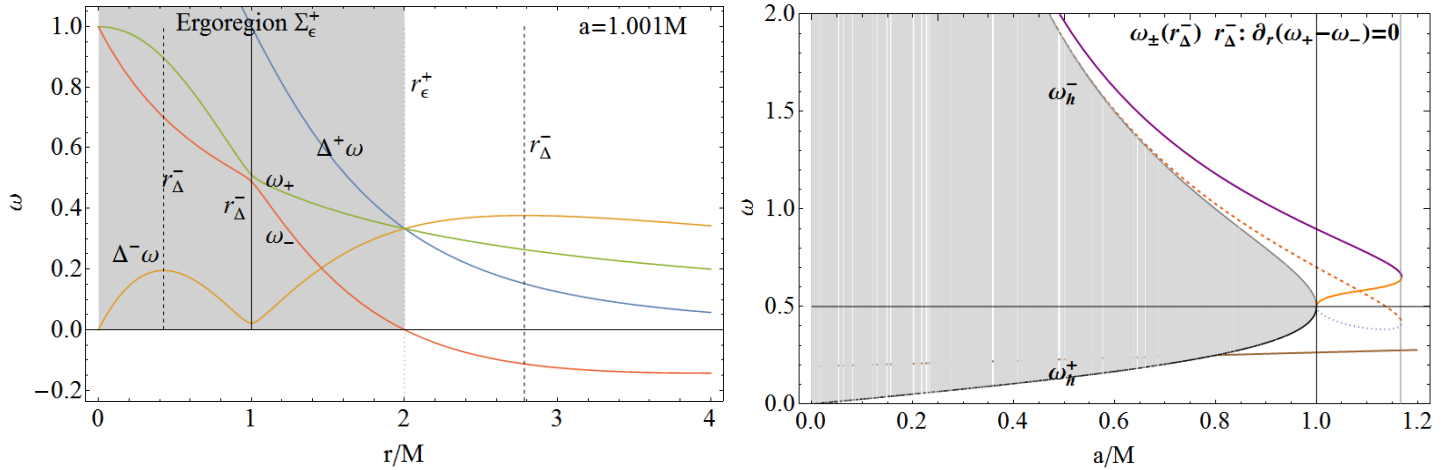


FIG. 7: Right panel: Plane $\omega - r$ for a **NS** with spin $a = 1.001M$. The plots are for the frequency difference $\Delta^{-}\omega \equiv \omega_{+} - \omega_{-}$, the sum $\Delta^{+}\omega \equiv \omega_{+} + \omega_{-}$, and the Killing bottleneck for the surfaces ω_{\pm} . The radii r_{Δ}^{-} and critical points of the ω_{\pm} are also shown. Note the role of the static limit r_{ϵ}^{+} and the r_{Δ}^{-} in the bottleneck definition. Right panel: Curves ω_{\pm} on r_{Δ}^{-} , i.e., solutions of $\partial_r \Delta^{-}\omega = 0$.

The bundles $g_{\bar{\omega}}$ contain an (almost) continuum and infinite set of metric parameter values a/M . Each value of a/M sets a specific Kerr geometry. From Fig. 8, it is clear that eventually some bundles contain both **BHs** and **NSs** spacetimes, others define only **BHs**, while none of the bundle is constituted by **NS** only. In fact, *all* the metric bundles are tangent at least in one point to the horizons a_{\pm} . Thus, from the quantities (15) an alternative definition of **BHs** Killing horizons r_{\pm} emerge. Indeed, from Fig. 8, it follows that the horizons a_{\pm} arise as the envelope surfaces of the curves $a_{\omega}^{\pm}(r)$, i.e., the metric bundles $g_{\omega} = a_{\omega}^{\pm}|_{\omega}$ in π_a . This will be a crucial property of the metric bundles with significant consequences that allow us to connect **NSs** to **BHs** in the extended plane. In fact, since the curve a_{\pm} is tangent to all metric bundles g_{ω} , the (inner and outer) horizons contain all the frequencies ω defining each metric bundle and, therefore, describing both **NSs** and **BHs** in the extended plane.

From Fig. 8, it follows that a metric bundle has its *origin* a_0 on the vertical axis $r = 0$ of π_a and closes on the tangent point to a_{\pm} . The closeness of the metric bundles is due to the spacetime rotation. To investigate the solutions (15), which define the closed bundles, we solve the condition $a_{\omega}^{+} = a_{\omega}^{-}$ and find

$$a_{\omega}^{+} = a_{\omega}^{-} \quad \text{on} \quad \frac{r_{\partial}^{\pm}(\omega)}{M} = \pm \frac{\sqrt{\omega^2 + 1}}{\omega} - 1 \quad \text{where} \quad a_{\omega}^{\pm}(r_{\partial}) \equiv a_{\partial} = 2\omega r_{\partial} \quad \text{and} \quad (16)$$

$$a_{\omega_{\partial}}^{+} = \frac{2M\sqrt{r}}{\sqrt{r+2M}} = 2r\omega_{\partial}^{+} \quad \text{where} \quad \omega_{\partial}^{+} = \frac{M}{\sqrt{r(r+2M)}}.$$

The frequency ω_{∂}^{+} of Eq. (16) is a solution of the equation $r_{\partial}^{+} = r$ (see Fig. 10); the function $\omega_{\partial}^{+}(r)$ is, therefore, the frequency associated to the orbits r_{∂}^{+} , where $a_{\omega}^{+} = a_{\omega}^{-}$ defines the metric bundle. In fact, $\omega_{\partial}^{+}(r)$ does not depend on the spacetime spin because the information on the corresponding geometry can be extracted from π_a through r_{∂}^{+} , i.e.,

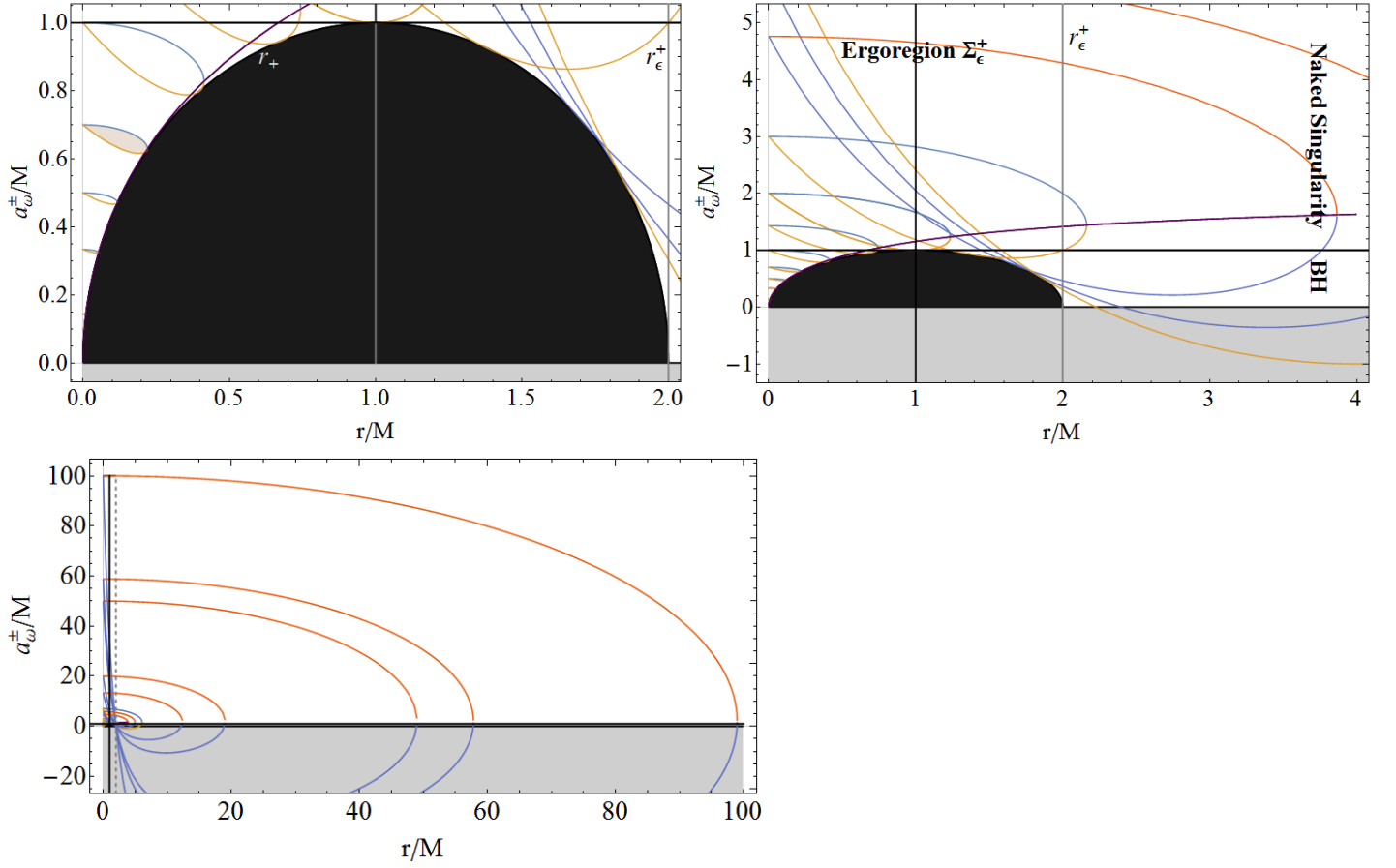


FIG. 8: Spins a_ω^\pm versus r/M for different frequencies. The black region is for $r < r_+$ and r_+ is the **BH** outer horizon. See also Fig. 9 for a 3D representations of these regions.

from the condition $a_\omega^+ = a_\omega^-$. Consequently, ω_∂^+ is a function of the radius $r = r_\partial^+$. The pairs $(r_\partial^+, \omega_\partial^+(r))$ identify the corresponding spin origin a_0 (also origin of the metric bundle), which is defined by the frequencies $\omega_\partial^+(r)$ and $a_\omega^+ = a_\omega^-$ at r_∂^+ —Fig. 10. Asymptotically, for very large values of r/M , the value $\omega_\partial^+ = 0$ is approached as shown in Fig. 8, where $a_\omega^+ = a_\omega^-$ is valid on the line $a = 0$, that is, approaching the limiting geometry of the static and spherically symmetric Schwarzschild spacetime.

We note that r_∂^- is negative for positive values of the frequency. As we are restricting our analysis in this work to the case $\omega > 0$, we shall not consider r_∂^- ; nevertheless, an analysis of the case $\omega < 0$ would, in fact, provide additional information about the spacetime structure even in the equatorial plane. A very small ω_∂^+ , on the other hand, corresponds to a very large (origin) spin $a_0 = M/\omega$. Note that the spin a_0 corresponds to the frequency $\omega_0 = M/a$, which was introduced in Eq. (8) by considering the behavior of the stationary observer frequencies near the singularity $r = 0$; this is of importance in **NS** geometries as described in Sec. III. The properties of this special frequency ω_0 have also been extensively discussed in [18]. More generally, as noted in Secs. II and III, the dimensionless spin parameter a/M is related to the quantity M/ω through the frequencies of the light surfaces (see [18]). Then, the function $a_{\omega_\partial^+}^+(r)$ in Eq. (16) is obtained as $a_\omega^\pm(r, \omega_\partial^+)$. As shown in Fig. 10, the condition $a_{\omega_\partial^+}^+(r) = a_\pm$ is valid only at the spacetime singularity $r = 0$; otherwise, $a_\pm < a_{\omega_\partial^+}^+(r) < 2M$, while the condition $a_{\omega_\partial^+}^+(r) = 2M$ (a **NS**) is reached asymptotically for large values of r/M .

Note that the asymptotic limit of $a_{\omega_\partial^+}^+(r) = 2M$ is relevant as it corresponds to a metric bundle g_ω^\pm at constant frequency $\omega = 0.5$, which defines the point of the envelope corresponding to the extreme Kerr **BH** solution $a = M$. Figure 12 refers to the analysis of Fig. 8 and sketch the correspondence between **BHs** and **NSs** derived from the analysis of a_ω^\pm . The envelope a_\pm of the a_ω^\pm curves is defined as the set of points $(a/M, r/M)$ for which $\partial_\omega a_\omega^\pm = 0$, i.e., as the curve tangent to all a_ω^\pm or also as the boundary of the region filled by the curves a_ω^\pm . Then, small changes of a and shifts along the orbit radius r leave ω almost constant as a_ω^\pm are continuum functions.

The relation between the radius r_∂^\pm , the spin a_∂^\pm and frequencies ω_\pm has to be confronted with Eq. (12) for the

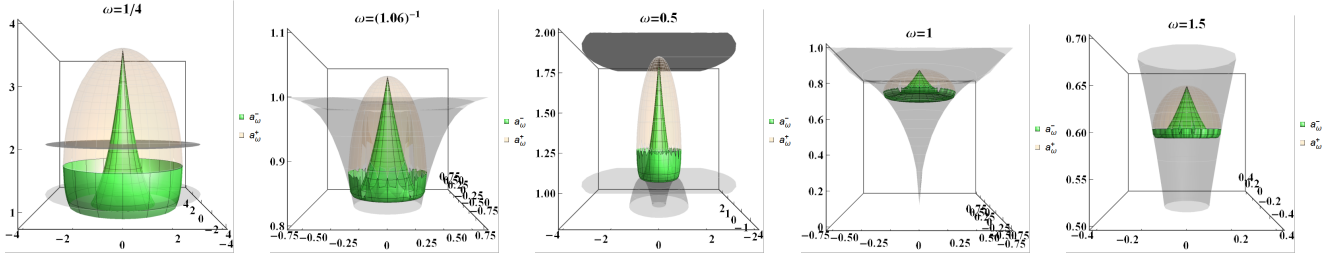


FIG. 9: Kerr geometries: Surfaces a_ω^\pm (in units of mass) versus the radius r/M for different frequencies ω , including **BH** and **NS** geometries—see also Eq. (15). 3D representations of a_ω^\pm versus r/M for different frequencies—see also Fig. 8. Each surface is a metric bundle g_ω for a fixed value of $\omega_0 = \text{constant}$. The corresponding metric bundle origin is $a_0 = M/\omega_0$. The surfaces a_ω^\pm are represented as revolution surfaces with height a_ω^\pm (vertical axes) and radius r/M (horizontal plane). Surfaces are generated by rotating the two-dimensional curves a_ω^\pm around an axis (revolution of the function curves a_ω^\pm around the “z” axis). Thus, $a = \text{constant}$ with respect to the radius r/M is represented by a circle under this transformation. The disks in the plots are either $a = M$ or $r = r_\epsilon^+ = 2M$. The surfaces a_ω^\pm are green and pink colored, respectively (as mentioned in the legend). Horizontal surfaces determined by $a_\pm = \sqrt{r(2M - r)}$ are gray surfaces. For each fixed frequency $\omega = \bar{\omega}$ there is an associated spin $\bar{a} \equiv \bar{\omega}^{-1}$ (see the discussion in Sec. IV). In the **BH** range, the surfaces a_ω^\pm are in the region $r < r_-$, where r_- is the inner horizon.

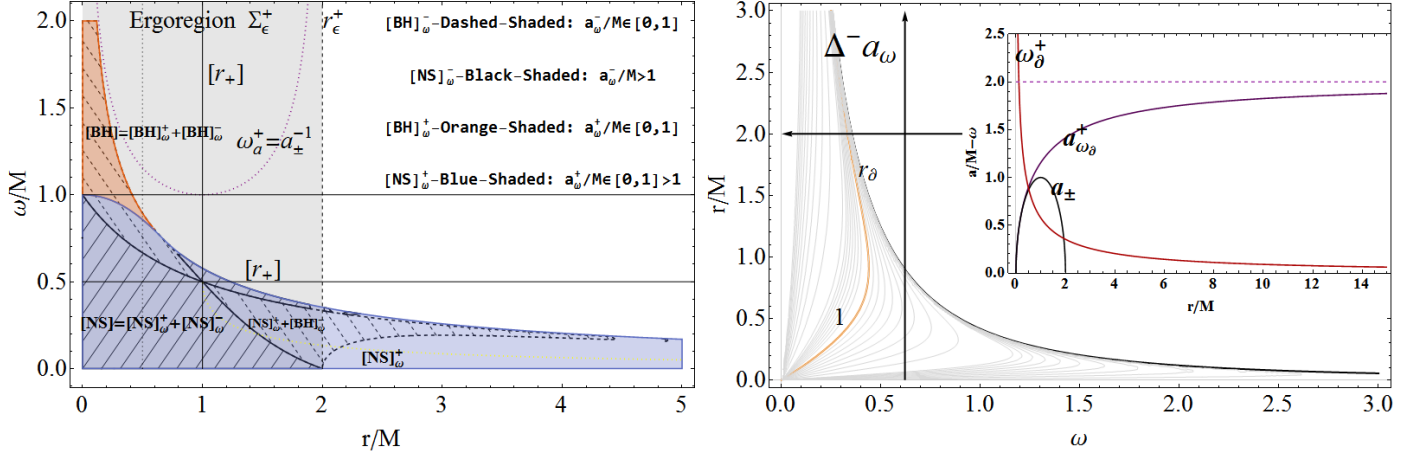


FIG. 10: Left panel: Regions $a_\omega^\pm > M$ (**NS**) and $a_\omega^\pm \in [0, M]$ (**BH**) versus r/M . The ergoregion Σ_ϵ^+ , the **NS** and the **BH** regime are shown. Right panel: $\Delta^- a_\omega \equiv a_\omega^+ - a_\omega^- = \text{constant}$ in the plane $r - \omega$. The arrows indicate increasing values of $\Delta^- a_\omega$. The curve $a = M$ and $r_\theta(\omega)$ are shown. Inside panel: The frequency ω_θ^+ , spins $a_\pm = \sqrt{r(r - 2M)}$, which define the **BHs** horizons and $a_{\omega_\theta}^\pm$ defined in Eq. (16) as functions of r/M .

frequencies ω_H^\pm at the horizons and radii r_\pm of the **BH** Killing horizons. These quantities play an important role also for the Killing bottleneck emergence considered in Sec. III, as the surfaces $a_\omega^\pm(\omega) = \text{constant}$ are related to the solutions $\omega_\pm(a)$ of Eq. (8) and shown in Fig. (11). The relation $r_\pm^\pm \omega = a_\omega^\pm/2$ of Eq. (16) is also used in Fig. 12 to unveil some **BHs** and **NSs** properties: The points on the lines $a_0 = \text{constant}$ for $a_0 \in]M, a_\bullet]$ lead to the Killing bottleneck emergence of Fig. 11.

BHs and NSs in metric bundles g_ω

As discussed above, a metric bundle g_ω can comprise only **BHs** or **BHs and NSs**. Moreover, the horizons describe **BHs and NSs** in the extended plane. In the remaining of this section, we describe this last aspect and the **BHs-NSs** relation more closely.

Firstly, Fig. 10-left represents **BHs** and **NSs** in the $\omega - r$ plane. The plane is divided into regions, where the metric bundles g_ω include **BHs** or **NSs**; there are regions with only **BHs** or **NSs** and transition regions that cross different sections and are connected to Killing horizons and bottlenecks—see also Fig. 11. A special transition region is, for example, around the extreme **BH** horizon $r = M$ with frequency value $\omega = 1/2$, which corresponds to the extreme Kerr **BH**.

We concentrate on the restricted $\pi_a^+ \subset \pi_a$ plane determined by $a \geq 0$ in Figs. 8. The restriction of the extended plane π_a to π_a^+ exploits the symmetry by reflection around the axis $a = 0$, where negative origins of metric bundles build up the horizons $-a_\pm < 0$. The plane has the following remarkable sections: \mathcal{P}_S , \mathcal{P}_L , \mathcal{P}_\odot , \mathcal{P}_H , and \mathcal{P}_\otimes . The

line $\mathcal{P}_S = (r = 0, a = \text{constant})$ includes **BHs** and **NSs**. \mathcal{P}_S represents the collection of all origins a_0 . A variation of the dimensionless spin of the singularity (at $r = 0$) corresponds to a variation of a_0 in \mathcal{P}_S . This line also represents the singularity frequencies $\omega_0 = M/a_0$. Moreover, we define $\mathcal{P}_L = (r_\partial, a_\partial)$ and the set $\mathcal{P}_H = (a_\pm, r)$ for the Killing horizons. Curves a_ω^\pm at constant ω closes on \mathcal{P}_L and have origins in \mathcal{P}_S . The line $\mathcal{P}_\odot = (a = 0, r)$ describes the limiting case of the Schwarzschild solution. \mathcal{P}_\odot crosses \mathcal{P}_H in $r = 0$ and $r = 2M$. Finally, the set $\mathcal{P}_\otimes = (a = M, r)$ describes the extreme Kerr spacetime and crosses \mathcal{P}_H at $a_\pm = M$ and $r = M$. The collection of all the points $a_\omega = \text{constant}$ generates the light-curves shown in Fig. 11, where the Killing bottleneck and Killing throat emerge at $a_\omega/M > 1$.

According to Fig. 8, metric bundles can be classified in two classes. **(1)** The first class includes the curves a_ω^\pm tangent to r_- , including those bundles which are “entirely” contained in the **BH** sector of π_a^+ , i.e., $a \in [0, M]$ and $r \in [0, r_-]$. **(2)** The second class includes metric bundles tangent to the outer horizon r_+ , containing **BHs** and **NSs** in the same bundle. These two classes are separated by the limiting bundle g_ω^\pm with origin $a_0 = 2M$ and tangent to the maximum of a_\pm ; that is, the point in π_a^+ with $r = M$, for $a = M$ and frequency $\omega = 0.5$, describing the extreme Kerr spacetime. Bundles with origins in the **BH** sector are *completely* contained in an “inaccessible” region between the singularity, $r = 0$, and the inner horizon r_- . Bundles with origin in the the naked singularity sector $a > M$ comprise **BH** and **NS** geometries, which are, therefore, related because they are contained in the same metric bundle. (Notice that the definition of g_ω^\pm , through the stationary observers definition, provides a **BH-NS** relation). The case of very strong **NSs** (very large a/M , asymptotic value $a \approx +\infty$) corresponds to the limiting point $r_+ \approx 2M$ and $a \approx 0$ —see Fig. 8. This suggests that the **NS** sector is closely related to the **BH** sector. We explore this connection more deeply below.

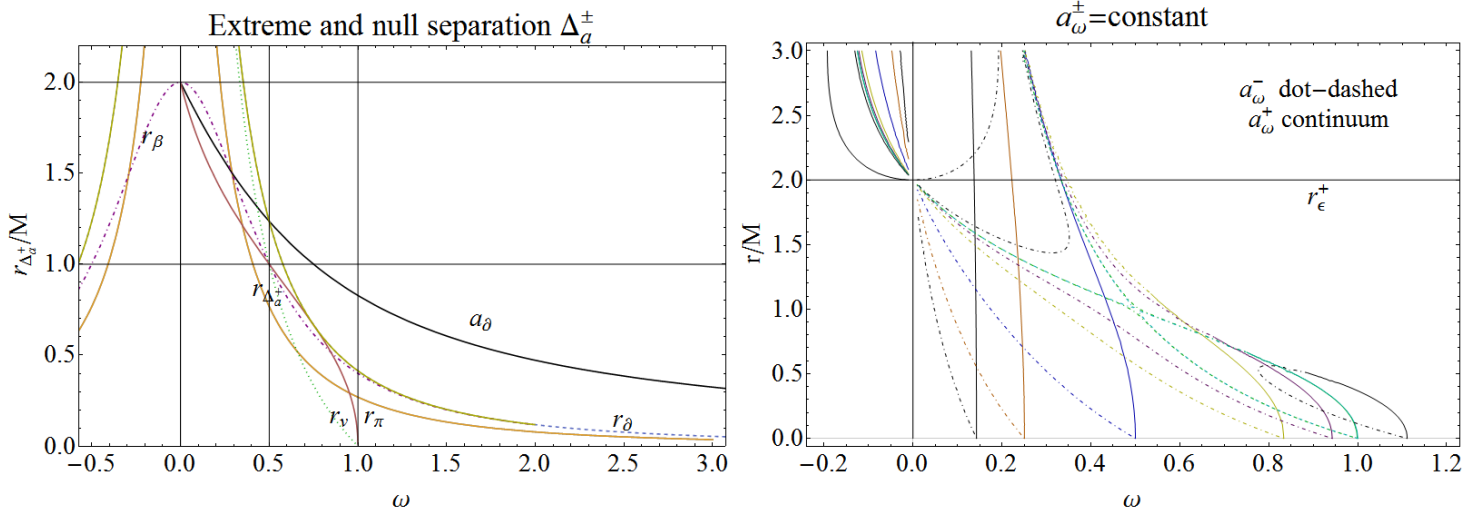


FIG. 11: Left panel: Radii $\{r_\Delta, r_\beta, r_\delta, r_\nu, r_\pi\}$ and the spin a_δ , according to the Eqs. (B5), (16) and (B1), as functions of the frequency ω . Left panel: Spins $a_\omega^\pm = \text{constant}$ given in Eq. (15) in the plane $r/M - \omega$. Coalescence of the Killing horizons r_+ and r_- in the extreme black hole geometries and the emergence of a Killing throat and Killing bottleneck in the **NS** geometries are shown—see also Figs. 2,1,27,28 and 26. Here $\Delta^\pm a = a_\omega^\pm \pm a_\omega^-$. The radius r_δ satisfies the equation $\Delta^- a = 0$. The radii $r_\Delta \equiv r_\Delta^\pm : \partial_r \Delta^\pm a = 0$, and $\{r_\beta, r_\nu, r_\pi\}$ are limiting radii.

The horizons as an envelope surface of the metric bundles

An important consequence of the approach presented here is that it allows us to establish a relation between **BHs** and **NSs**. In fact, the outer horizon in π_a^+ emerges as an envelope surface of metric bundles with only **NSs** origins. That is, the **BH** outer Killing horizon r_+ relates a **BH** with $a \in [0, M]$ with a **NS** with $a \in]2M, \infty]$. The inner horizon in π_a^+ can be constructed by metric bundles with **NS** and **BH** origins. Viceversa, the **BH** horizons are tangent to all the metric bundles. All the **BHs** and **NSs** frequencies ω_\pm are, therefore, related to the horizon frequency ω_H , and all horizon frequencies are the limiting orbital photon frequencies in **NS** and **BH** spacetimes—Figs (8). As the horizon is tangent to all the metric bundles, each metric bundle is defined by one frequency ω , which coincides with the horizon frequency ω_H on the tangent point in the extended plane. Frequencies ω in (15) are actually the limiting frequencies ω_\pm . It follows that the metric bundles, connected the singularities frequencies ω_0 , are defined by the origins of the metric bundles and the horizon frequencies ω_H .

Remarkably, the construction of the *inner* horizon r_- is confined to metric bundles contained entirely in the **BH** sector. This fact could lead to important consequences, when considering the collapse towards a **BH** and the process of formation of the inner horizon. These metric bundles are all confined in the π_a^+ region $r \leq r_-$ and $a \leq M$. This

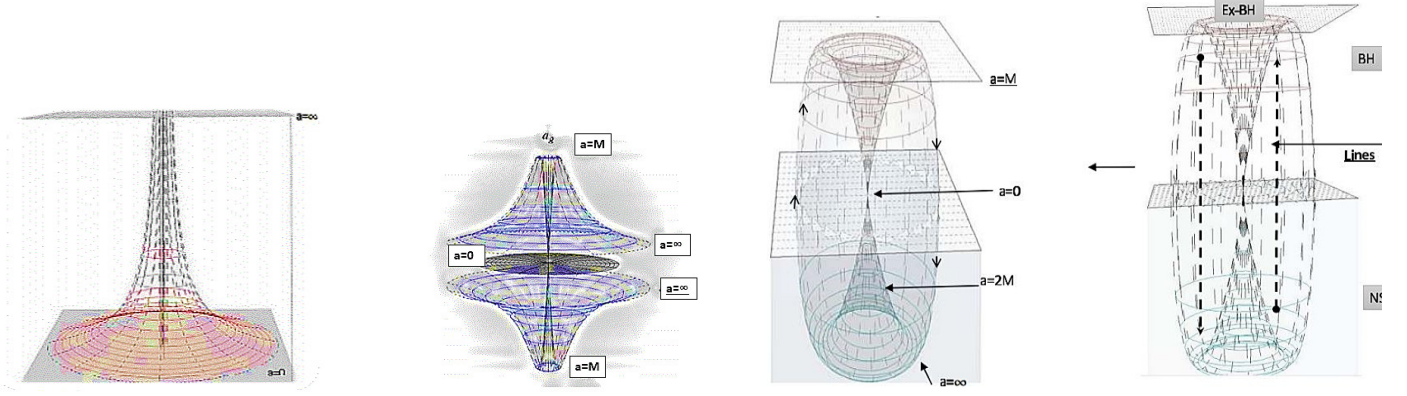


FIG. 12: Schematic representation of the **BHs-NSs** correspondence. See also the $a_g(a_0)$ function of Fig. 13. Right first panel: The spin $a = 2M/\omega$ between the planes $a = 0$ and $a = \infty$ — cf. Eq. (12). Third and fourth panels: Representation of the **BHs-NSs** correspondence. An own-up-arrow indicates the relation **NS-BH**, defining the outer horizon r_+ . An up-down arrow determines the inner horizons, which are totally included in the **BH**. The limiting cases $a = 0$, $a = M$, $a = 2M$ and $a = \infty$ are also shown.

implies that the inner horizon $r_-(\bar{a})$ of a **BH** with spin \bar{a} is related to a metric bundle with origin a_0 in the **BH** or **WNS** ($a \in [M, 2M]$) regions, while the outer horizon $r_+(\bar{a})$ is related to a **NS** metric bundle.

Before continuing, it is convenient to return to the concept of metric bundle, as shown in Fig. 8, and analyze three particular curves in detail: **(1)** the horizontal lines $a = \text{constant}$ of π_a ; **(2)** the vertical lines $r = \text{constant}$ and; **(3)** the curves a_{\pm} corresponding to horizons.

(1) The horizontal lines $a = \text{constant}$

For a **BH** or a **NS** with $a_0 \in \mathcal{P}_S$, there are two curves a_{ω}^{\pm} of the bundle, which are tangent at a point $p \in \mathcal{P}_H$ on the horizons. Each metric bundle $g_{\omega}^{\pm}(a_0)$ is associated to a constant frequency, $\omega_0 = M/a_0$, defined by the bundle origin a_0 . Considering a bundle, there is a pair of points $p_1(a) = (a, r_1(a))$ and $p_2(a) = (a, r_2(a))$ with $a = \text{constant}$ and $r_1(a) < r_2(a)$, which are located respectively on the two curves of the bundle. A special case is the pair of points present on the origin line, \mathcal{P}_S , where $r_1(a_0) = r_2(a_0) = 0$. Also the horizons \mathcal{P}_H for the extreme Kerr spacetime are special. Note that, in general, the condition $r_1(a) < r_2(a)$ on the horizon for $a = a_H \in a_{\pm}(r)$ leads to Eq. (13). On the orbits $(r_1(a), r_2(a))$, light-like orbital frequencies ω_{\pm} are equal to $\omega_a(r_1) = \omega_a(r_2) = M/a$, where $\omega_a \in (\omega_+, \omega_-)$. There are two special geometries associated to the closure points \mathcal{P}_S and \mathcal{P}_H : \mathcal{P}_S represents the singularity $r = 0$ with $\omega_a(0) = \omega_a(0) = M/a$, corresponding to a spacetime with spin a . Moreover, the second special geometry is always a **BH**, whose (inner or outer) horizon has the frequency $\omega_H = M/a$, i.e., the frequency of the bundle. We investigate the spin a_g of this specific spacetime below.

We note that metric bundles cross each other in π_a^+ . This means that, in a fixed spacetime with a fixed radius, there are two limiting frequency values ω_{\pm} . Therefore, the maximum number of crossing points between metric bundles is two. Consequently, there are two crossing metric bundles with origins at $a = 1/\omega_{\pm}$, respectively.

(2) Vertical lines $r = \text{constant}$.

Let us now focus on the vertical lines in π_a^+ and the intersections on each metric bundle. For a fixed orbit r , there are, in general, two Kerr geometries corresponding to the spins $a_1(r) < a_2(r)$ of the same bundle. In addition, there are the following limiting cases: 1. At $r = 0$ there is an infinite number of origins, where $a_1(0) = a_2(0)$ on a bundle. 2. The point r_t is the tangent point of the vertical line to the bundle, satisfying the condition $a_{\omega}^+(r_t) = a_{\omega}^-(r_t)$ — see Eq. (16) and Fig. 10. The condition $r_{\partial}^{\pm} = r_{\pm}$ is satisfied only in special geometries a_R . In general, for $r \in]0, r_{\partial}^+[,$ there are two geometries $a_1 < a_2$, corresponding to two **BHs** or one **BH** and one **NS**. This implies that at a fixed r , there are two geometries (a_1, a_2) with frequencies $\omega = 1/a$. The case of the geometries identified in the extended plane by the vertical lines will be clarified at the end of this section because it is necessary to consider the tangency conditions as shown in Fig. 17. With respect to this property, $a_1 < a_2$, there are two exceptions represented by the metric bundles with vertical lines tangent to the horizon. There are two asymptotic cases, where $a_1 = a_2$; these cases with respect to the horizon points $(a = 0, r = 0)$ and $(a = 0, r = 2M)$ correspond to the limit of the Schwarzschild spacetime— Fig. 17. In general, a vertical line $r = \bar{r}$ on a metric bundle g_{ω_0} defines two geometries with $\omega_+ = \omega_0$ and $\omega_- = \omega_0$. More details on this point will be addressed at the end of this section. In other words, this property relates limiting frequencies of different spacetimes. This result is in agreement also with the results presented in Sec. III.

(3) The horizon surfaces a_{\pm}

All the metric bundles have the frequencies $\omega_H = 1/a_{\pm}$ at the horizon in the extended plane. As the metric bundle

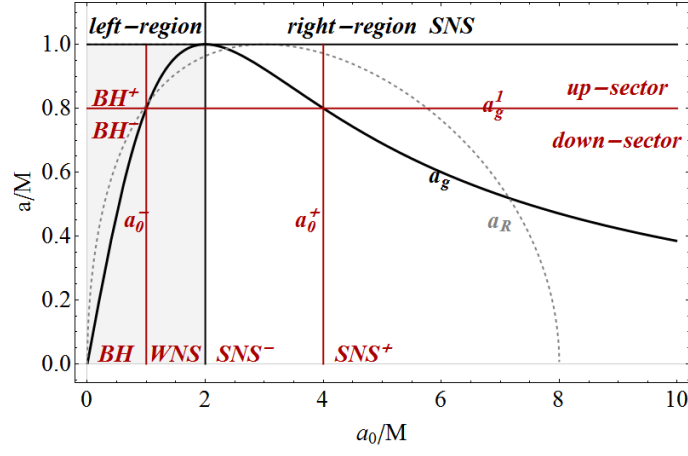


FIG. 13: Plots of the spins a_g and a_R defined in Eq. (17) as functions of the origin a_0/M . **BH** and **NS** regions are gray shaded. a_g is a representation of the **BHs-NSs** correspondence –see also Figs. 12. The sectors and regions corresponding to strong naked singularities (**SNS**) and weak naked singularities (**WNS**) are explicitly shown (cf. definitions given in Sec. IV). Here $a_0^- = M$, $a_0^+ = 4M$: $a_g = a_g^+$, $a_g^1 = (3/4)M = a_g(a_0^-)$.

frequency ω_0 is also a limiting photon orbital frequency ω_+ or ω_- and as all frequencies ω_0 represent also the horizon frequency ω_H , then the limiting photon frequencies ω_{\pm} on an orbit r in all the spacetimes $a \in [0, \infty[$ are the horizons frequencies ω_H in the extended plane. Viceversa, the set of the horizon frequencies ω_H in the extended plane is the collection of all the limiting orbital photon frequencies ω_{\pm} in any **BH** or **NS** spacetime. This issue will be discussed in detail below.

BHs-NSs correspondence

The relation between **BHs** and **NSs** can be formalized by introducing the functions $a_g(a_0)$ and $a_R(a_0)$ of the origin a_0 as follows

$$\forall a_0 > 0, \quad a_g \equiv \frac{4a_0M^2}{a_0^2 + 4M^2} \quad \text{where} \quad a_g \in [0, M] \quad \text{and} \quad \lim_{a_0 \rightarrow 0} a_g = \lim_{a_0 \rightarrow \infty} a_g = 0, \quad a_g(a_0 = 2M) = M, \quad (17)$$

$$\text{and} \quad a_R(a_0) \equiv \sqrt{4\sqrt{(a_0 + M)MM} - (a_0 + 4M)M}. \quad (18)$$

The behavior of these functions is plotted in Figs. 13. For a fixed value of the origin a_0 , the function $a_g(a_0)$ defines univocally the outer r_+ or the inner r_- horizon. This relation includes the Schwarzschild limiting case, which corresponds to the limit $a/M \rightarrow +\infty$, and the extreme Kerr spacetime, which is connected with the naked singularity value $a = 2M$ —see also Figs. 12. More precisely, $a_g(a_0)$ is the solution of the equations $a_{\omega}^{\pm}(r_{\pm}, \omega_0) = a$, where $\omega_0 = M/a_0$ —while $a_R(a_0)$ is the solution of the equations $r_{\partial}(a_0) = r_{\pm}$, providing information about the orbits where the curves a_{ω}^{\pm} close at the horizons. The analysis of off-equatorial and charged generalizations considered in Sec. V reaffirms this result. According to Figs. 8, each point r_H on the horizon is univocally related to a **NS** or a **BH** metric in the π_a^+ plane. Each frequency ω is in correspondence with a point r_H on r_- or r_+ . In this sense, we might say that the information contained on the horizon (the frequency ω_H) is extracted by the functions a_{ω}^{\pm} .

Furthermore, it is immediate to see that from the expression $a_g(a_0)$ of Eq. (17), we obtain a relation between the horizon tangent spin (horizon frequency) and the bundle origin (bundle frequency), namely, $\omega_0^{-1} \equiv a_0^{\pm}/M = \frac{2r_{\pm}(a_g)}{a_g} \equiv \omega_H^{-1}(a_g)$; in particular, from $\omega_0^{-1} \equiv a_0^{\pm}/M = \omega_H^{-1}(a_g)$, it is seen that the bundle frequencies ω_0 represent all (and only) the horizon frequencies on the tangent point, i.e., $\omega_H(a_g(a_0)) = \omega_0$. This implicitly relates also the horizons frequencies with the singularity frequencies; there are then particular **BH** spacetimes, where the outer horizon r_+ or the inner and outer horizon r_{\pm} are defined by bundles with **NSs**. We detail this aspect below. Here we note that there is only one fixed point for the transformation $a_g(a_0)$, namely $a_0 > a_g$, and $a_0 = a_g$ for $a_0 = 0$.

We now introduce the concept of couples of related metric bundles, say, **BD** and **BC** (see Fig. 14). In the first couple, the first bundle has its origin in the **NS** region (tangent to the outer horizon) and the second bundle is completely or partially contained in the **BH** region (tangent to the inner horizon). The two bundles with origins (a_0, a'_0) share equal tangent spin a_g . That is, if $a_0 > a'_0$, then the bundle with origin a_0 , frequency $\omega_0 = Ma_0^{-1}$, has the contact spin a_g in $r_g \in r_+$ with horizon frequency $\omega_H^+(r_g, a_g) = \omega_0 = Ma_0^{-1}$. The second bundle of the couple has its origin at a'_0 , frequency $\omega'_0 = M/a'_0$, tangent spin a_g in $r'_g \in r_-$ and horizon frequency $\omega_H^-(r'_g, a_g) = \omega'_0 = M/a'_0$.

Bundles g_{ω_0} and $g_{\omega'_0}$ determine, in the sense of the envelope surface, respectively, the outer horizon $r_+ = r_g$ and the inner horizon $r_- = r'_g$ of the **BH** spacetime with spin a_g . The relation between the tangent points (a_g, r_g) and the origin a_0 and the relations between **BHs** and **NSs** through the bundles will be addressed in full details below. Importantly, the condition of the bundle correspondence, i.e., $a_g(a_0) = a_g(a'_0)$, leads to the non-trivial solution $a'_0 = a_p \equiv 4M^2/a_0$ (see **DD** and **BB** model bundles of Figs. 14, 15, and 16 and Tables III and II). In terms of the horizon frequency (equal to the bundles frequencies), there is $\omega'_0 = \frac{1}{4\omega_0}$; in fact, using Eq. (12), this relation can be written in compact form as $\omega_H^+ \omega_H^- = \frac{1}{4}$ (or we can write $a_0^+(a_g) a_0^-(a_g) = 4M^2$), which is independent of the spin a , in general. In Fig. 14, the solutions $a_0^\pm/M = \frac{2r_\pm(a_g)}{a_g}$ correspond to $a = a_0$ and $a = a_p$.

In the second couple, **BC**, the origin spin of one bundle a'_0 is the tangent point $a_g(a_0)$ of the second bundle with origin a_0 (therefore, a'_0 is always a **BH** and the other bundles are all **BHs**). An example of these couples are the models **BB** and **CC** of Figs. 14, 15, and 16 and Tables III and II.

To enlighten some properties of the **BC** and **BD** bundles, we consider the difference $G[a_0] \equiv (a_0 - a_g)$ as a function of a_0 and the recurrence relation for a_g , i.e., $a_g[n+1] = \frac{4a[n]M^2}{a[n]^2 + 4M^2}$ where $a[0] = a_0$. Then, $a_g[n+1]$ decreases with the cycle order n (see Fig. 14). In fact, in **BC** bundles, the cycles are confined to the inner horizon in the extended plane (apart from the starting point a_0). Naturally, the only fixed point, $a_p = a_0$, of this relation is in $a_0 = 2M$, corresponding to the extreme **BH**.

Bundles **BD** have coincident cycles and bundles **BC** have partially coincident cycles; therefore, **BD** and **BC** bundles are related by partially coincident cycles (see Table II and Fig. 14).

TABLE II: Recurrence relation $a_g[n]$ for different starting points, see also Fig. 14. **BD** bundles with coincident cycles (**BB** and **DD**) are clearly denoted (excluding the initial point) and partially coincident cycles in **BC** bundles are also shown. Cycles (with the exclusion of the initial point a_0) are entirely confined in the **BH** region. Models **XX** where $\mathbf{X} = \{\mathbf{A}, \mathbf{B}, \mathbf{C}, \mathbf{D}\}$ are defined in Fig. 15.

a_0	$a_g[1]$	$a_g[2]$	$a_g[3]$	$a_g[4]$	$a_g[5]$	$a_g[6]$	$a_g[7]$
1 (BB)	0.8	0.689655	0.616366	0.562903	0.521586	0.48837	0.460889
2 (CC)	1.	0.8	0.689655	0.616366	0.562903	0.521586	0.48837
4 (DD)	0.8	0.689655	0.616366	0.562903	0.521586	0.48837	0.460889
1/2 (AA)	0.470588	0.445902	0.424787	0.406451	0.39033	0.376008	0.363172
$a_p(1/2)=8$	0.470588	0.445902	0.424787	0.406451	0.39033	0.376008	0.363172
$a_g(1/2)=0.470588$	0.445902	0.424787	0.406451	0.39033	0.376008	0.363172	0.351579

To conclude this analysis, we note that it is possible to find a linear relation between the horizons curves (in the extended plane) by re-expressing the curve of the inner horizon as a function of the outer horizon (on the lines $a = \text{constant}$) and, viceversa, i.e., $r_-(r_+)$ and $r_+(r_-)$ —Fig. 14.

BH-NS correspondence: one-to-one relation

There is a one-to-one correspondence between the points of the horizons, the horizon frequencies, and the spins $a \in [0, \infty[$ for **NSs** or **BHs**. **BHs** are related to a part of the r_- curve, **SNSs** ($a > 2M$) correspond to r_+ , and **WNSs** ($a \in [M, 2M]$) are in correspondence with the envelope surfaces of the inner horizon, i.e., $a_- \in \pi_a^+$ for $r \in [0.8M, M]$. The limiting cases of Schwarzschild, $a = 0$, and extreme Kerr **BH**, $a = M$, are connected with the limit $a = \infty$ and the double point $a_0 = 2M$, respectively.

In fact, we can say that $\forall \bar{a} \in]0, +\infty[, \exists ! \bar{\omega}_0 \equiv M/\bar{a}$ and, *viceversa*, $\forall \bar{\omega}_0$ there is *one and only one* $a_0 \in]0, M]$: $\bar{\omega}_0 = \omega_H$, where ω_H is the horizon frequency, i.e., we connect points of \mathcal{P}_S to points of \mathcal{P}_H of the horizons by considering that each metric bundle relates univocally an origin a_0 of \mathcal{P}_S with a tangent point of \mathcal{P}_H . (a_g is solution of $a_0 = \omega_H^{-1}$). Any origin of the metric bundle $g_{\omega_0}^\pm$, associated to a frequency $\omega_0 = \text{constant}$, is associated to one and only one point p_\pm : $p_- \in r_-$ or the outer $p_+ \in r_+$, according to the origin a_0 .

A special case is the extreme Kerr **BH** solution, where the origin spin $a_0 = 2M$, associated to the metric bundle g_{ω_0} of constant frequency $\omega_0 = 1/2$, crosses the horizons at $r_\pm = M$ and $a_\pm = M$. In general, for a fixed origin a_0 , there are two frequencies ω_H and $\omega_0 \equiv M/a_0 \neq \omega_H$, respectively, where $\omega_0 = M/a_0$ is the frequency of the metric bundle g_{ω_0} , and $\omega_H \neq \omega_0$ is the horizon frequency defined by the spin a_\pm defined by the tangent point. $p_\pm \equiv (a_\pm, r_\pm) \in \pi_a^+$.

The one-to-one **BHs-NSs** correspondence is described by the function a_g as given in Eq. (17) and illustrated in Fig. (13). We can say that each **BH** solution is connected to one and only one **NS** in π_a^+ , as it emerges from the analysis of the Killing horizons and light frequencies on the equatorial plane and, viceversa, each **NS** is related to one **BH**. These considerations include the limiting cases of the Kerr extreme spacetime, where the associated metric bundle has origin $a_0 = 2M$, and the limiting case of the static Schwarzschild **BH**, which is connected to the **NS** with $a = +\infty$. The **BH-NS** relation allows us to consider a spin shift from an initial **BH**₁ (**NS**₁) source as corresponding to a shift of the respective **NS**₁ (**BH**₁); therefore, the pair **BH**₁ – **NS**₁ shifts to the pair **BH**₂ – **NS**₂. The segment

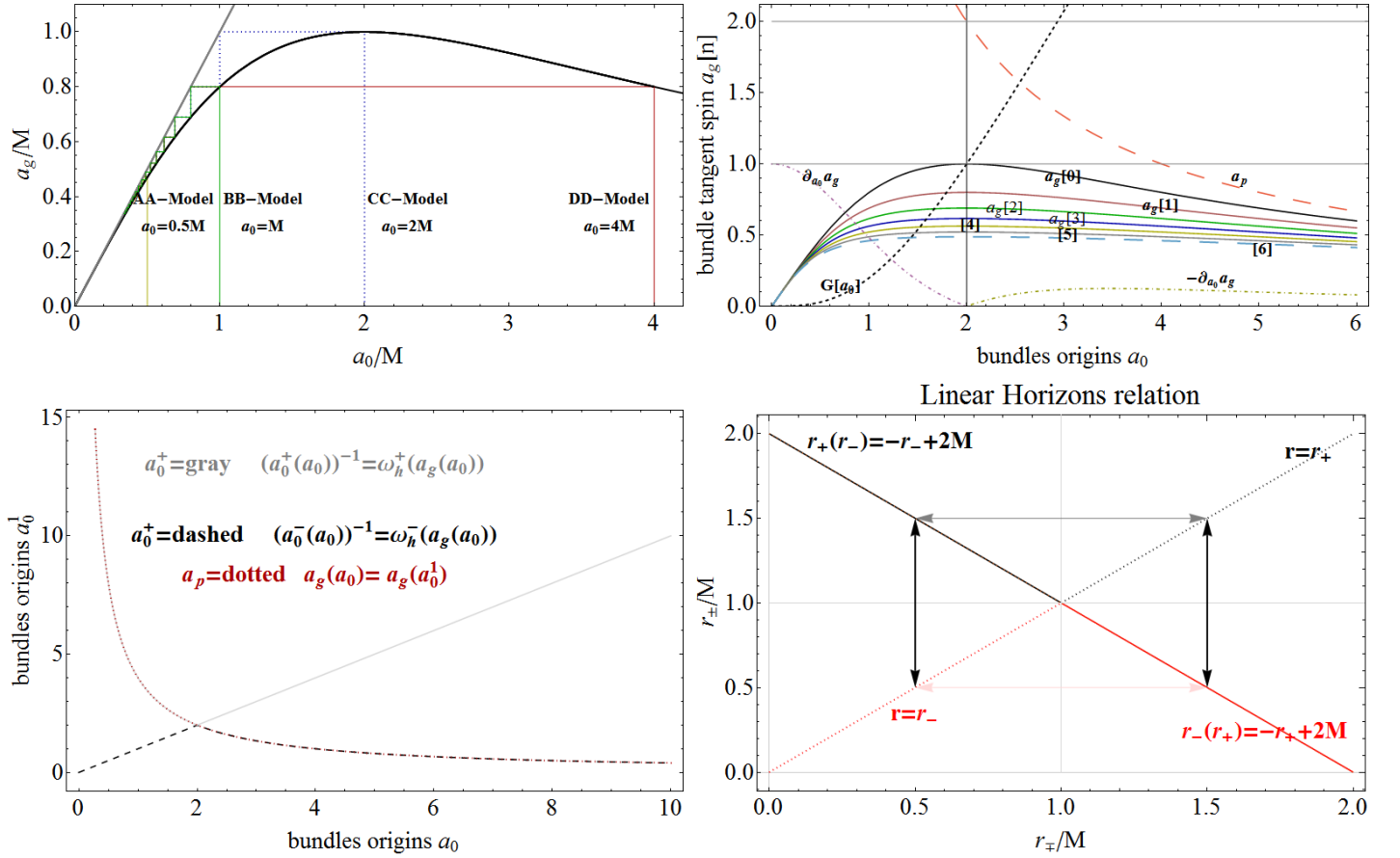


FIG. 14: Below right panel: The functions $r_-(r_+)$ (red line) and $r_+(r_-)$ (black line) (on the lines $a=\text{constant}$ of the extended plane). The region $r_\pm \times r_\mp \in [0, 2M] \times [0, 2M]$ describes **BH** horizons in the extended plane along the red and black lines or, equivalently, the dotted lines, according to the symmetries enlightened in the plot. Below left panel: The solutions $a_0^\pm/M = \frac{2r_\pm(a_g)}{a_g}$ as functions of bundle origin a_0 ; they correspond to $a = a_0$ and $a = a_p$, i.e., $a_g(a_0) = a_g(a_p)$ and $\omega_0^{-1} \equiv a_0^\pm/M = \frac{2r_\pm(a_g)}{a_g} \equiv \omega_H^{-1}(a_g)$, determining the related **BC** or **BD** bundles—Table II. Upper panels: Recurrence relation for the point $a_g[n]$ as function of the starting points a_0 . **BD** bundles have coincident cycles (**BB** and **DD**) with the exception of the initial point; **BB-CC** bundles have partially coincident cycles. Cycles (with the exclusion of the initial point a_0) are entirely confined in the **BH** region. Models **XX** with $\mathbf{X} = \{\mathbf{A}, \mathbf{B}, \mathbf{C}, \mathbf{D}\}$ are defined in Fig. 15. For a fixed a_0 , $a_g[n]$ decreases with the number of cycles. The importance of the bundle with origin $a_0 = 2M$ is also shown; this is related to the extreme Kerr BH and there is a maximum for each cycle; $a_0 = 2M$ is the fixed point of the transformation $a_0 = a_p$. The difference $G[a_0] \equiv a_0 - a_g$ increases reaching $G[2M] = 1M = 2M - a_g$ only for the first cycle—Table II.

$a_{\text{BH}_1} - a_{\text{NS}_1}$ of $\mathcal{P}_S \in \pi_a^+$ transforms into $a_{\text{BH}_2} - a_{\text{NS}_2}$, becoming larger or smaller depending on the curve a_g as shown in Fig.13.

To conclude this section, we analyze the relation between the tangent radius r_g on the horizon and the bundle origin a_0 . We start with a description of Fig. 13.

Analysis of Figure 13

Figure 13 represents the spin $a \in \text{BH}$ versus a_0 . Spins $a \in \text{BH}$ and a_0 are connected through a_g . The sectors and regions in this figure are determined by the following special boundary spins, considering that $a_0 \in [0, +\infty]$ and $a_g \in [0, M]$:

- the origin $a_0^- = M$ distinguishes **NSs** from **BHs**;
- the spin $a_0 = 2M$ defines the *left region* where $a_0 \in [0, 2M]$ (for **BH** and **WNS**) and *right region* where $a_0 > 2M$ (for **SNSs** = **SNS**⁻ \cup **SNS**⁺);
- the spin $a_g^1 \equiv a_g(a_0^-) = 0.8M$ defines the *up-sector* where $a \in [a_g^1, M]$ (for **BH**⁺) and the *down sector* where $a \in [0, a_g^1]$ (for **BH**⁻);
- the spin $a_0^+ = 4M$: $a_g = a_g^+$ distinguishes strong naked singularities **SNS**⁺ and **SNS**⁻.

Consequently,

- a bundle origin a_0 in the **BH**-region corresponds through the horizon curve to **BH**⁻ singularities ($a_g : a_0 \in \mathbf{BH} \mapsto a_g \in \mathbf{BH}^-$);
 - origins a_0 in the **WNS**-region correspond to $a_g \in \mathbf{BH}^+$.
- Therefore, $a_g \in \mathbf{BH} = \mathbf{BH}^- \cup \mathbf{BH}^+$ correspond, through the tangency with the inner horizon curve a_- , to $a_0 \in \mathbf{BH} \cup \mathbf{WNS}$;
- the origin a_0 in **SNS**⁻ corresponds to $a_g \in \mathbf{BH}^+$;
 - the origin a_0 in **SNS**⁺ corresponds to $a_g \in \mathbf{BH}^-$.
- Therefore, $a_g \in \mathbf{BH} = \mathbf{BH}^- \cup \mathbf{BH}^+$ is related to $a_0 \in \mathbf{SNS}^- \cup \mathbf{SNS}^+$.

Because $\partial_{a_0} a_g \geq 0$, increasing the origin spin $a_0 \in \mathbf{BH} \cup \mathbf{WNS}$ and the tangent spin $a_g \in \mathbf{BH}^- \cup \mathbf{BH}^+$ increases the *left region*. Let us consider the **BHs** and **NSs** correspondence determined by the tangent point spin a_g . Note that a fixed origin $a_0 \in \mathbf{SNS}^+$ (down-right region) corresponds to the outer horizon tangent point (we identify $a_g(a_0) \in \mathbf{BH}$). This is sufficient for the determination of the spin $a_0^- \in \mathbf{BH}^-$ and the origin of the bundle metric tangent to the inner horizon in (a_g, r_g^-) ; therefore, this defines the inner horizon r_g^- of the **BH**⁻ spacetime with spin a_g .

Similarly, in the *right-up* region there are couples following related geometries (a_g, a_0) : (1) **BH**⁺ – **WNS** and (2) **BH**⁺ – **SNS**⁻.

We note that the origins **SNS**[±] (a_0) are in correspondence with a $a_g \in \mathbf{BH}$; also the $a_0 \in \mathbf{WNS}$ and $a_0 \in \mathbf{BH}$ are in correspondence with a $a_g \in \mathbf{BH}$.

Therefore, in general there is a correspondence $a_0 \mapsto a_g \in \mathbf{BH} \mapsto a'_0$, i.e, the origin of the bundle defines a tangent point to the horizon a_g and r_+ or r_- in the spacetime with a_g ; correspondingly, there is the bundle with origin a'_0 whose tangent point to the horizon is a_g and r_- or r_+ , respectively.

Therefore, the following triple relations hold

$$\underbrace{[a_0 \in \mathbf{SNS}^+ \mapsto a_g \in \mathbf{BH}^- \mapsto a'_0 \in \mathbf{BH}]}, \quad \underbrace{[a_0 \in \mathbf{SNS}^- \mapsto a_g \in \mathbf{BH}^+ \mapsto a'_0 \in \mathbf{WNS}]}; \quad (19)$$

(a) (b)

$$\underbrace{[a_0 \in \mathbf{WNS} \mapsto a_g \in \mathbf{BH}^+ \mapsto a'_0 \in \mathbf{SNS}^-]}, \quad \underbrace{[a_0 \in \mathbf{BH} \mapsto a_g \in \mathbf{BH}^- \mapsto a'_0 \in \mathbf{SNS}^+]} \quad (20)$$

(c) (d)

The geometries of the triple relations given in Eq. (19) are bounded together by $a_0 \in a_+$ and the inner horizon r_- ; on the other hand, the geometries of the two relations in Eq. (20) are bounded together by $a_0 \in a_-$. The geometries of the last two triple relations are bounded by a_g . The sets ((b) and (c)) and ((a) and (d)) are related by an exchange of spins a_0, a'_0 . Bundles corresponding to the tangent $a = a_g$ (same tangent point spin) belong to triplets connected by arrows. We shall see this also below considering some examples—see also Table II.

The black hole area, delimited by the (outer) horizon, is a crucial quantity, determining the thermodynamic properties of **BHs**. Given the relevance of this concept, we study in Sec. (B) some properties of the areas of the regions delimited by metric bundles and compare them with the horizon area $\mathcal{A}_{r_\pm}^\pm = \pi/2$ in the extended plane π_a^\pm , i.e., the region in the plane π_a^\pm bounded by the horizon curve a_\pm .

To conclude, we show that the horizons frequency ω_H defines the bundles frequencies. We will resume part of the discussion carried out in relation with Eq. (17). We also investigate the limiting frequencies obtained from the bundles crossing and some properties of the tangents to the horizons in the extended plane.

On the frequencies

The bundle frequency is a limiting photon-like frequency, ω_+ or ω_- as introduced in Sec. (II), at the point (a, r) of the bundle. The second, limiting photon frequency at the point (a, r) , ω_- or ω_+ , respectively, is determined by the bundles crossing. As previously discussed, there is a maximum of two bundles at the intersection. This second frequency is, therefore, the solution of $a_{\omega_1}^\pm(\bar{r}) = a_{\omega_2}^\pm(\bar{r})$, where ω_1 is the known frequency of the bundle g_{ω_1} , \bar{r} is a fixed point of the bundle. The second photon frequency ω_2 , identifying the related bundle g_{ω_2} , is a function of ω_1 and \bar{r} :

$$a_{\omega_1}^+ = a_{\omega_2}^\pm : \quad \text{for } \omega_1^{(+,\pm)} = \omega_- \quad (21)$$

$$a_{\omega_1}^- = a_{\omega_2}^- : \quad \text{for } \omega_1^{(-,-)} = \omega_+ \quad \omega_\pm \equiv -\frac{(r-2) \left[(r^2+4) \omega_2 \pm 4\sqrt{r^2 \omega_2^2 [1-r(r+2)\omega_2^2]} \right]}{16r^3 \omega_2^2 + (r-2)^2 (r+2)}. \quad (22)$$

The solutions $a_{\omega_1}^\pm$ for $\omega_2 = \text{constant}$ are shown in Fig. 15. Note that the limiting curve for the constant frequencies curves $\omega_1^{(+,\pm)}, \omega_1^{(-,-)}$ is r_∂^+ of Eq. (16)—see also Fig.10,11.

By definition, the frequency ω is constant along the bundle; thus, the bundle frequency ω is the bundle origin frequency $\omega_0 = M/a_0$ and, particularly, the frequency at (a_g, r_g) , where a_g is the bundle spin at the tangent point r_g on the horizon curve. We can show that the bundle frequency coincides with the horizon frequency at the tangent point r_g , that is, $\omega_0 = \omega_H(a_g, r_g)$.

First, note that the bundle frequency $\omega = \omega_0$ is defined in $[0, \infty]$. The analysis of the frequency variation domain gives us indications that both the inner ω_H^- and outer horizon frequency ω_H^+ define the bundle frequency, as there is $\omega_H^+ \in [0, 1/2]$ and $\omega_H^- \in [1/2, +\infty[$ (for $a \in [0, M]$)—see also Fig. (1). Then, condition $\omega_0 = \omega_H$, where ω_H is the union $\omega_H^+ \cup \omega_H^-$, leads to $a_g(a_0)$, relating the tangent-point-spin a_g and the bundle origin $a_0 = \omega_H^{-1}(a_g)$.

Fig. III and Table 15 show some notable numerical examples, proving that the bundle frequencies are, in fact, the horizon frequency at the tangent point to the horizons. Connections between the two bundles g_{ω_1} and g_{ω_2} at equal a_g , which are related to the horizons points $r_{\pm}(a_g)$, are also shown in Table 15. The tangent spin a_g can be also obtained from the relation $a_{\omega}(r_{\pm}, \omega_0) = a$ by solving for $a_0(a)$ and representing the result as $a_g(a_0)$ in Eq. (17).

Then, we can consider the bundle on the horizon ($r = r_g$) with the bundle frequency ω expressed as the origin frequency $\omega = \omega_0$. In terms of frequencies, from $\omega_H = \omega$, we obtain $a = 4\omega_*/(4\omega_*^2 + 1)$, where $\omega_* \in [0, 1/2]$ for $\omega_H = \omega_H^+(r_+) = \omega_*$, and $\omega_* \geq 1/2$ for $\omega_H = \omega_H^-(r_-)$. This shows also the role of the inner horizon frequency. This relation can be also found from the spin $a_g(a_0)$, where $a_0 = \omega_0^{-1}$. Note that we can eliminate the frequency ω from a_{ω}^{\pm} of Eq. (15) and parametrize the metric bundles in terms of a and r , using the condition $\omega = \omega_H$ in a_{ω}^{\pm} . In this case, there is $a \in [0, M]$ as the spin is the horizon tangent-point spin a_g :

$$a_{\omega}^{(\natural)}(\omega_H^b) \equiv (\natural) \frac{\sqrt{a^2 r^2 [8r_b - a^2(r(r+2) + 4)] + (\natural) a r_b}}{a^2(r+2)}, \quad (\natural) = \pm; \quad b = \mp. \quad (23)$$

The bundles $a_{\omega}^{(\natural)}(\omega_H^b)$ are, therefore, parameterized for the tangent point $a = a_g$ —see Fig. 15. From the condition of coincidence between bundle and horizon in the extended plane (i.e., $a_{\omega}^{\pm} = a_{\pm}$), we obtain $r = \frac{2}{4\omega_*^2 + 1}$ and assuming $r = r_{\pm}$, then $\omega = \omega_H$.

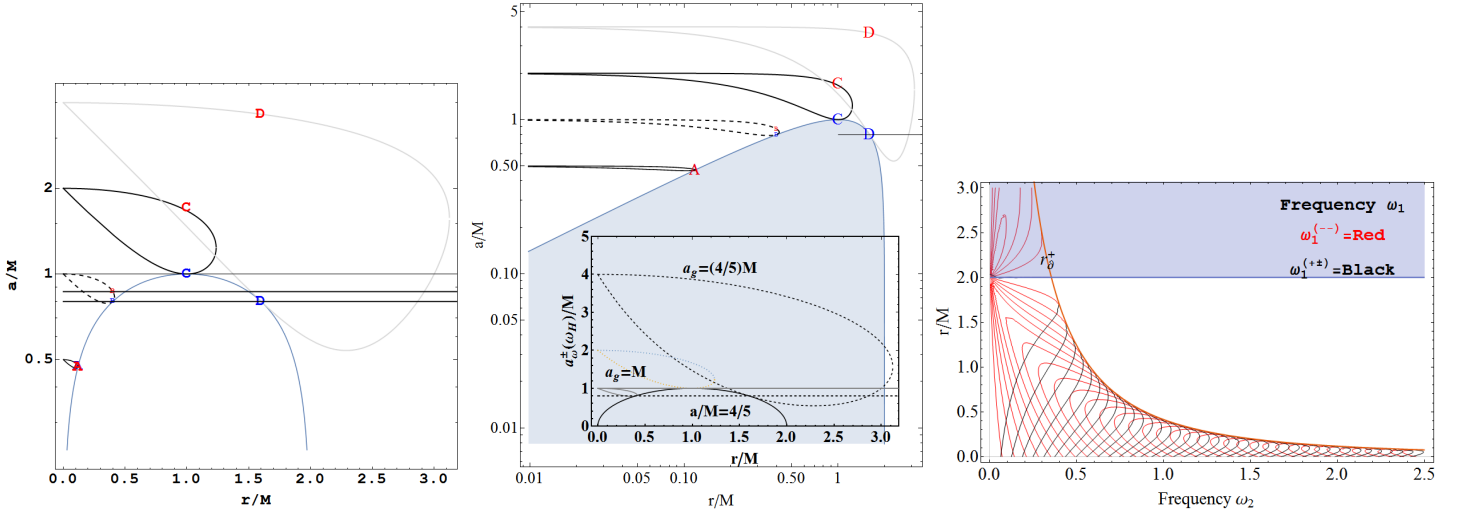


FIG. 15: *Left and center panels:* Models \mathbf{XX} where $\mathbf{X} = \{\mathbf{A}, \mathbf{B}, \mathbf{C}, \mathbf{D}\}$ considered in Table III. The spin a_{ω} as a function of r/M for different origins a_0 with tangent point (r_g, a_g) on the horizon curve. The spins $a_g < a_g^o$ are represented on $\mathbf{X}^i < \mathbf{X}^o$, where $a_g^o(\mathbf{X}^o)$ corresponds to the outer spin of the bundle for $r = r_g$. $\mathbf{X} = \mathbf{A}$: origin $a_0 = 1/2$, frequency $\omega = 2$; $\mathbf{X} = \mathbf{B}$: $a_0 = 1$, $\omega = 2$; $\mathbf{X} = \mathbf{C}$ $a_0 = 2$, $\omega = 1/2$; $\mathbf{X} = \mathbf{D}$ $a_0 = 4$, $\omega = 0.25$. The bundle D is related to C as $a_g(\mathbf{D}) = a_g(\mathbf{B})$. The model \mathbf{D} (\mathbf{B}) defines $r_+(a_g)$ ($r_-(a_g)$) for the BH spacetime with spin $a = a_g$. (*Center panel:*) Shaded region is delimited by the horizon curve. Models \mathbf{XX} are shown. Inside panel: bundles parameterized in terms of the horizon frequency ω_H of Eq. (23) are shown with a_g values. *Right panel:* The shaded region is $r > r_{\epsilon}^+ = 2M$. Frequencies $\omega_1 = \text{constant}$ of Eqs. (21)-(22) in terms of the frequencies ω_2 and r .

On the tangent lines

A relevant aspect of the metric bundle is that it is tangent to the horizon the extended plane. The tangent line with respect to the horizon is horizontal only for extreme Kerr BH (where the line $a = \text{constant}$ has a double contact point on the tangent bundle) and asymptotically vertical in the static case. To study the tangents at the horizon, we

TABLE III: Models **XX**, where $\mathbf{X} = \{\mathbf{A}, \mathbf{B}, \mathbf{C}, \mathbf{D}\}$ as defined in Fig. 15.

Models:	AA-Model	BB-Model
Bundle frequency:	$\omega_0 = 2$	$\omega_0 = 1$
Tangent point r_g :	$r_g = 2/17$	$r_g = 2/5 \in r_-$
Bundle spin a_g at r_g :	$a_g = 0.470$ $a_\omega^+(r_g) = 0.474 (A^\circ > A^i)$	$a_g = a_\omega^-(r_g) = 4/5 (\mathbf{D})$ $a_\omega^+(r_g) = 13/15 (B^\circ > B^i)$
Horizon frequency ω_H at r_g :	$\omega_{\mathbf{H}}(\mathbf{r}_g, \mathbf{a}_g) = 2 \equiv \omega_0$	$\omega_{\mathbf{H}}(\mathbf{r}_g, \mathbf{a}_g) = 1 \equiv \omega_0$
Bundle frequency for r_+ or r_- :	$\omega_{\mathbf{H}}^+(r_g, a_g) = 1/8$	$\omega_{\mathbf{H}}^+(r_g, a_g) = 1/4 (D_i)$
Horizon frequency (X°):	$\omega_{\mathbf{H}}^-(r_g, a_\omega^+(r_g)) = 1.984$ $\omega_{\mathbf{H}}^+(r_g, a_\omega^+(r_g)) = 0.126$	$\omega_{\mathbf{H}}^-(r_g, a_\omega^+(r_g)) = 0.865$ $\omega_{\mathbf{H}}^+(r_g, a_\omega^+(r_g)) = 0.289$
Models:	CC-Model	DD-Model
Bundle frequency:	$\omega_0 = 1/2$	$\omega_0 = 1/4$
Tangent point r_g :	$r_g = 1$	$r_g = 8/5$
Bundle spin a_g at r_g :	$a_g = 1$ $a_\omega^+(r_g) = 5/3 (C^\circ > C^i)$	$a_g = 4/5 (\mathbf{B})$ $a_\omega^+(r_g) = 3.644$
Horizon frequency ω_H at r_g :	$\omega_{\mathbf{H}}(\mathbf{r}_g, \mathbf{a}_g) = 1/2 \equiv \omega_0$	$\omega_{\mathbf{H}}(\mathbf{r}_g, \mathbf{a}_g) = 1/4 \equiv \omega_0 (B_i)$
Bundle frequency for r_+ or r_- :	$\omega_{\mathbf{H}}^-(r_g, a_g) = 1 (\mathbf{B})$	
Horizon frequency (X°):	\emptyset	\emptyset

consider the variations⁵ $\partial_r a_\pm = (M - r)/\sqrt{-(r - 2M)r}$, with a_ω^\pm in the form of Eq.(15) (or, alternatively, Eq. (23)). The tangent curve is:

$$a_{\text{tangent}}(r) \equiv \frac{r(M - r_g) + Mr_g}{\sqrt{-(r_g - 2M)r_g}} \quad \text{where } r_g \in [0, 2M], \quad (24)$$

and the tangent point r_g is a parameter.

The bundle-horizon tangent line at the point (r_g, a_g) is provided by the relation $\partial_r a_\omega^\pm = \partial_r a_\pm$, where a_\pm is the horizon curve in the extended plane. These solutions are shown in Fig. 16, where some properties of the tangents are highlighted.

The solution of the tangency condition $a_g = a_\pm$ leads to the functions r_g^{real} and r_g^\vee :

$$a_g = a_\pm : \quad \frac{r_g^{\text{real}}}{M} \equiv \frac{2a_0^2}{a_0^2 + 4M^2} \quad \text{and} \quad \frac{r_g^\vee}{M} \equiv \frac{8M^2}{a_0^2 + 4M^2}. \quad (25)$$

$$\text{Viceversa:} \quad \frac{r_g^\mp}{M} \equiv \frac{r_\mp(a_g)}{M} = 1 \mp \sqrt{\frac{(a_0^2 - 4M^2)^2}{(a_0^2 + 4M^2)^2}}. \quad (26)$$

Figure 17 shows that $(r_g^{\text{real}}, r_g^\vee)$ coincide with (r_g^-, r_g^+) . The functions $(r_g^{\text{real}}, r_g^\vee)$ and (r_g^-, r_g^+) reveal some properties enlightened in Table III and further interesting symmetry properties of the **NS-BH** correspondence. Fig. 17 shows the relation between the tangent point r_g on the horizon and the bundle origin a_0 . Moreover, it points out the correspondence between the two metric bundles g_{ω_0} and g_{ω_1} , with equal tangent spin a_g and with different origin in **BH** and in **NS**. As made explicit in Table III, such bundles are related to the construction of the inner and outer horizon $r_\pm(a_g)$ of the **BH** spacetime with $a = a_g$.

It is clear that r_g^{real} is a combination of r_g^\pm and provides the tangent point $r_g(a_0)$ for the origin a_0 . In fact, by fixing a_0 there is only one tangent point in r_g^{real} equal to r_g^- for $a_0 < 2M$, or else equal to r_g^+ for $a_0 > 2M$; however, the second point at a_0 on the curve r_g^\vee (shaded region) has no immediate meaning with respect to the bundle g_{ω_0} ; on

⁵ The definition of metric bundle, tangent to the horizon in the extended plane presented in this work, should not be confused with the definition of *bundle metric* and of the *tangent bundle* of a differentiable manifold in differential geometry. A *metric* on a *vector bundle* is a choice of smoothly varying inner products on the fibers. While the a *tangent bundle* **TM** could be defined as the disjoint union of tangent vectors in M . Although different in their definitions, it is clear that the concepts introduced in this analysis can be read in terms of *tangent bundles* in a differential manifold, providing a deep insight on the properties considered here. While it is not the goal of this work, it is worth noting that we may consider the horizon as a one-dimensional surface embedded in the extended plane considered as R^2 (including the reflection π_a^-). For a general and smooth curve $c(r)$ in R^2 , the associated tangent bundle may be seen as a regular surface in R^4 , written as $T(r, \epsilon) = [c(r), \epsilon c'(r)]$ with $\epsilon \in [-1, 1]$. The metric bundles identify at every point on the horizon a tangent vector. We study the tangent to the horizons and the metric bundles ending Sec. (IV).

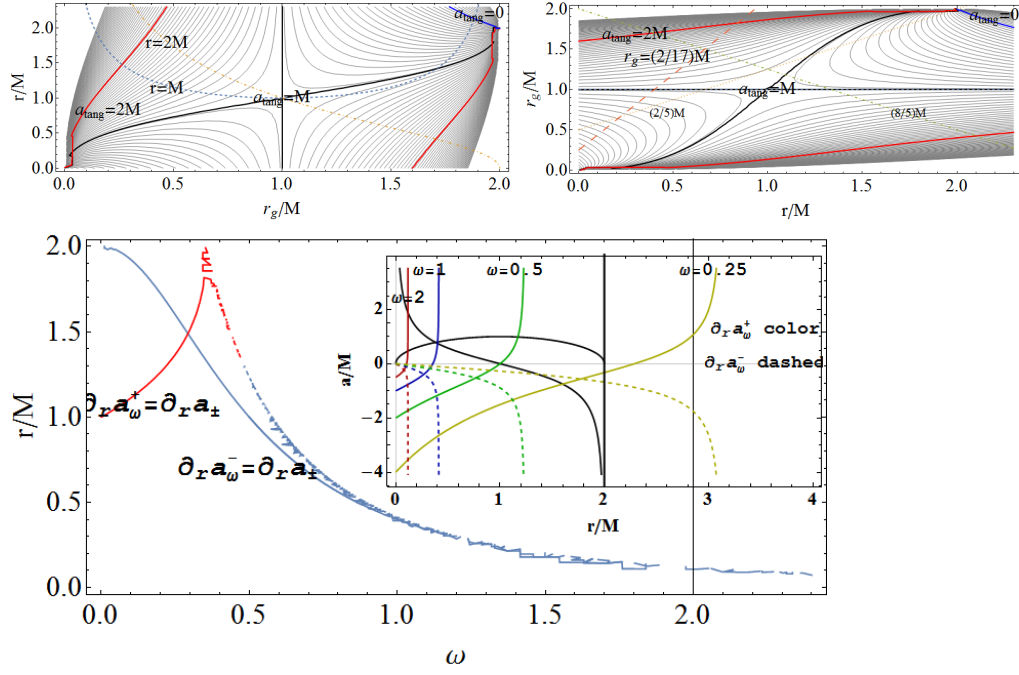


FIG. 16: Below panel: Solutions $\partial_r a_\omega^\pm = \partial_r a_\pm$ in the plane $r/M - \omega$. Bundles frequencies and the contact point to the horizons are represented for $\omega = 0.5$. The **CC** model of Fig. 15 and Table III, where $r_g = M$ and $a_g = M$. Inside panel: The black curve is the horizon a_\pm and the function $\partial_r a_\pm$; there are the two vertical asymptotes for the point $(a=0, r=0)$ and $(a=0, r=2M)$ corresponding to the limiting static geometry. Models **XX** are shown with bundle frequencies for the evaluation of $(\partial_r a_\omega^\pm(X))$, where $\mathbf{X} = \{\mathbf{A}, \mathbf{B}, \mathbf{C}, \mathbf{D}\}$ is considered in Table III and Fig. 15. Considering the models curves $(\partial_r a_\omega^\pm(X))$, their intersections with $\partial_r a_\pm$ provide the tangent point r_g and the tangent spin point a_g . Moreover, they indicate the bundle curve a_ω^+ or a_ω^- tangent to the horizon, as well as the tangent line inclination. *Upper panels:* $a_{tan} = \text{constant}$ in terms of (r, r_g) ; the black thick curve is $a_{tan} = M$; curves for some special values of the r and r_g are also shown. These are related to the models **XX**, where $\mathbf{X} = \{\mathbf{A}, \mathbf{B}, \mathbf{C}, \mathbf{D}\}$ is considered in Table III and Fig. 15.

the other hand, the point $r_g^\vee(a_0)$ provides the second horizon (r_- or r_+) in the spacetime with $a = a_g$. Therefore, the connecting bundle g_{ω_0} with g_{ω_1} is tangent to the horizon at $r_g^\vee(a_g)$. This case has been also represented in Table III with respect to the **BB** and **DD** models. Note that the **CC** model, extreme Kerr spacetime, corresponds to $a_0 = 2M$ and $r_g^{real} = r_g^\vee = M$ ($r_g^+ = r_g^- = M$).

We return to the analysis of (r_g^{real}, r_g^\vee) (r_g^\pm) in Fig. 17. Let us consider as an example the **BB** and **DD** models. For $a_0 < 2M$ the bundles are tangent to the inner horizon (note also the saddle point at $a_0/M = 2/\sqrt{3} \approx 1.1547$). According to the **DD** model $a_0 = 4M$, the correct tangent point is on $r_g^{real} = r_g^+$. The second point, for $a_0 = 4M$, on the $r_g^\vee = r_g^-$ is the tangent point $r_g(B)$ in the **BB** model with $a_0 = M$. The **BB** and **DD** models share same tangent spin a_g .

In conclusion, in this **BH** spacetime:

$$\begin{aligned} \text{the outer horizon is } r_+ &= r_g(D) = r_g^{real}(D) = r_g^+(D) = r_g^\vee(B) = r_g^+(B), \\ \text{the inner horizon is } r_- &= r_g(B) = r_g^{real}(B) = r_g^-(B) = r_g^\vee(D) = r_g^-(D). \end{aligned} \quad (27)$$

Consequently, we could say that $r_g^{real}(a_0)$ represents the horizon curve a_\pm as the envelope surface in the extended plane (note that asymptotically, for large values of a_0 , $r_g^{real}(a_0)$ approaches $2M$ from left). On the other hand, $r_g^\vee(a_0)$ provides information on the corresponding metric bundle and the second horizon for $a = a_0$. By using the couple (r_g^{real}, r_g^\vee) , it is sufficient the knowledge of the bundle origin to characterize the **BH** spacetime defined by the tangent bundle.

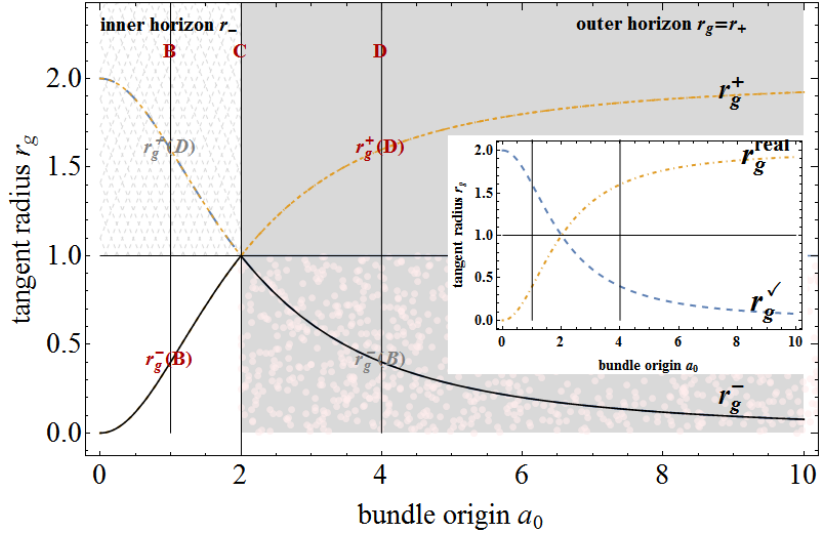


FIG. 17: Tangent radius r_g^\pm of Eq. (25) as a function of the tangent spin a_0 . Inside panel: (r_g^{real}, r_g^\vee) . The gray region represents SNS with $a_0 > 2M$ and the shaded regions are values of r_g^\vee . The models **XX** are also shown, where $\mathbf{X} = \{\mathbf{A}, \mathbf{B}, \mathbf{C}, \mathbf{D}\}$ is considered in Table III and Fig. 15.

V. THE KERR-NEWMAN GEOMETRIES

The investigation of Sec. (III) and Sec. (IV) is performed here for the case of Kerr-Newman (**KN**) and Reissner-Nordström (**RN**) spacetimes and in the region outside the equatorial plane of the Kerr spacetime. This further analysis will allow us to better evaluate the role of the frame-dragging. The analysis of Fig. 8 is presented in Fig. 20 for electrically charged geometries with $a = 0$. We prove that the closure of the metric bundles is a consequence of the rotation of the singularity: the correspondent curves, defining the **BHs** horizons for the static **RN** case, are open; the analysis of the **KN** case represented in Fig. 20 better shows the influence of the spin in the bending and separation into the two families of closed curves on the equatorial plane.

The Kerr-Newman geometry corresponds to an electro-vacuum axially symmetric solution with a net electric charge Q , described by metric (1) with $\Delta_{KN} \equiv r^2 + a^2 + Q^2 - 2Mr$. The solution $a = 0$ and $Q \neq 0$ constitutes the static case of the spherically symmetric and charged Reissner-Nordström spacetimes. The horizons and the outer and inner static limits for the **KN** geometry are respectively

$$r_\mp = M \mp \sqrt{M^2 - (a^2 + Q^2)}, \quad r_e^\mp = M \mp \sqrt{M^2 - a^2 \cos^2 \theta - Q^2}, \quad (28)$$

are depicted in Fig. 18. **KN** naked singularities are defined for $\mathcal{Q}_T^2/M^2 > 1$, where $\mathcal{Q}_T^2 \equiv (a^2 + Q^2)$ is the *total KN charge*. This condition implies that either $Q^2 > M^2$ or $a^2 > M^2$ give rise to a **NS**–[13–15]. Following Sec. (III), the frequencies $\omega_H^\pm \equiv \omega_\pm(r_\pm)$ at the horizons r_\pm are given by

$$\omega_H^- = \frac{aM \left(2M \sqrt{M^2 - (a^2 + Q^2)} - Q^2 + 2M^2 \right)}{4M^2 a^2 + Q^4}, \quad \omega_H^+ = \frac{aM}{2M \sqrt{M^2 - (a^2 + Q^2)} - Q^2 + 2M^2} \quad (29)$$

and are represented in Fig. 19. In this section, we consider the problem faced in the Secs. (III) and (IV) and analyze the entire range $Q^2 \geq 0$ and $a^2 \geq 0$. We test the conjectures presented in Sec. (IV) and reproduce the analysis of Sec. (III), in particular, for the case of spherical symmetry, when the frame-dragging due to the source’s spin is absent, isolating the effects of the electric charge from the rotation component of the total charge \mathcal{Q}_T . In doing so, we generalize the extended plane π_a^+ used in Secs. (III) and (IV), considering a two-parameter family of solutions and passing from the (1+1) dimensional problem of the Kerr spacetimes to a (1+2) problem of the **KN** solutions. Fixing one of the two components of the total charge, we can obtain an entire parametrized family of Einstein solutions. The off-equatorial case will also be briefly addressed.

In order to understand the effects of the two charge parameters a and Q , it is useful to look at the solutions (28) in the extreme cases. The axial symmetry of the metric is due to the presence of the spin of the central singularity. The presence of the electric charge actually “balances” the effects of the spin in several ways, as we shall see below.

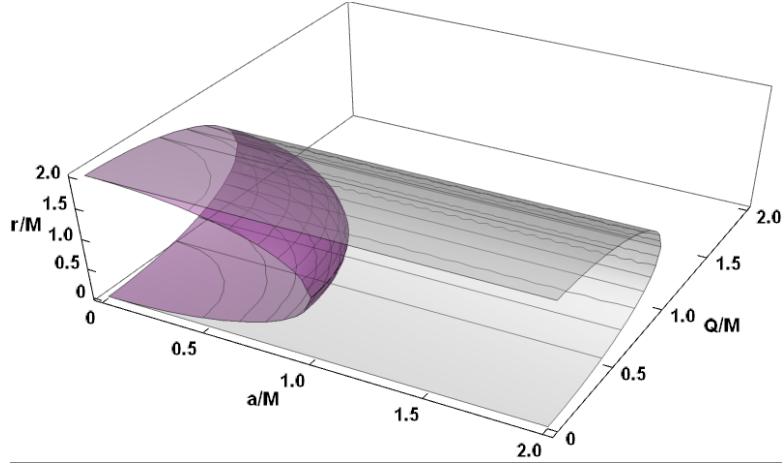


FIG. 18: Kerr-Newman solution—the equatorial plane. Plot of the horizons r_{\pm}/M (purple) and static limit r_{ϵ}^{\pm}/M (gray) as functions of a/M and Q/M —Eqs (28).

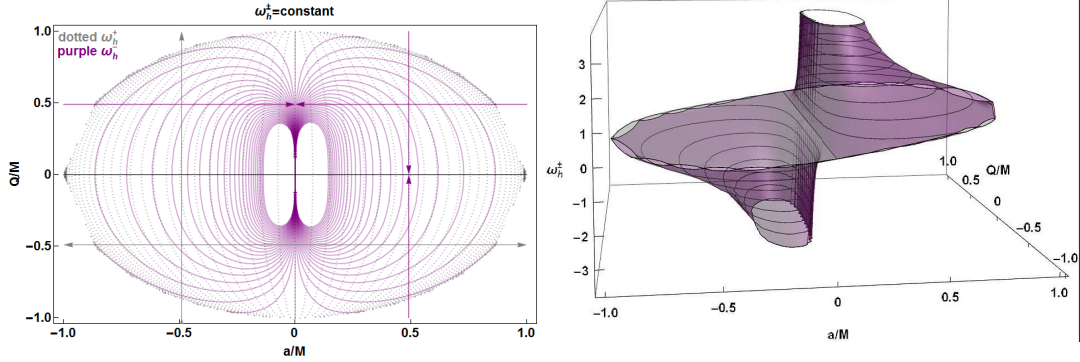


FIG. 19: Kerr-Newman spacetimes. The frequencies $\omega_H = \omega_{\pm}(r_{\pm})$ at the horizons r_{\pm} —see Eq. (29). *Left panel:* Curves $\omega = \text{constant}$. Arrows indicate the increasing magnitude of the frequencies ω_H^{-} (purple), ω_H^{+} (gray). *Right panel:* 3D plot of the frequencies ω_H^{\pm} as functions of the dimensionless spin a/M and charge Q/M .

In fact, we consider on the equatorial plane the static limits and the horizons of Eqs. (28) as follows

$$\text{static limits: } r_{\epsilon}^{\pm}|_{\theta=\pi/2} = M \pm \sqrt{M^2 - Q^2}, \quad \text{implying } Q/M < 1 \quad \text{or} \quad Q_{\pm}^{\epsilon} = \sqrt{-(r - 2M)r}; \quad (30)$$

$$\text{and } r_{\epsilon}^{\pm}|_{\theta=\pi/2} = M \quad \text{for } Q = M, \quad (31)$$

$$\text{BHs horizons: } a_{\pm} = \sqrt{-Q^2 - r(r - 2M)} \quad \text{or also} \quad Q_{\pm} = \sqrt{-a^2 - r(r - 2M)}. \quad (32)$$

Here, a_{\pm} and Q_{\pm} are solutions of $r_{\pm} = r$. On the equatorial plane, there are two static limits, independently of the spin, only for **KN BHs** or **NSs** having $Q < M$. In other words, the charge component of the **KN-NS** (and only for **NSs**) is not “predominant” with respect to the spin, i.e., for **KN-NSs** with $a \geq M$ but $Q < M$. On the equatorial plane, the static limits r_{ϵ}^{\pm} can be compared with the event horizons of the **RN BH** geometry, as in the Kerr geometry the static limit r_{ϵ}^{+} coincides the Schwarzschild horizon $r = 2M$. Conversely, this similarity appears even more clearly in the definition of Q_{\pm}^{ϵ} in Eq. (30), which is equal to the horizons a_{\pm} in the $a - r$ plane of the Kerr geometry. When $Q = M$, there is one static limit radius only, independently of the spin a/M . In this sense, the spacetime dragging is totally balanced, on the equatorial plane, by the electric charge $Q^2 > M^2$. For $(\theta \neq \pi/2, \theta \neq 0)$, a static limit exists provided the charge satisfies the condition $Q^2 \leq M^2 - a^2 \cos^2(\theta)$. On the other hand, for $Q = M$ ($a = M$) the Killing horizon is defined for $a = 0$ ($Q = 0$) only. The photon orbital frequencies in the **KN** geometry are

$$\omega_{\mp} = \frac{aM (Q^2 - 2Mr) \mp M \sqrt{r^4 [a^2 + Q^2 + (r - 2M)r]}}{a^2 [r(r + 2M) - Q^2] + r^4}. \quad (33)$$

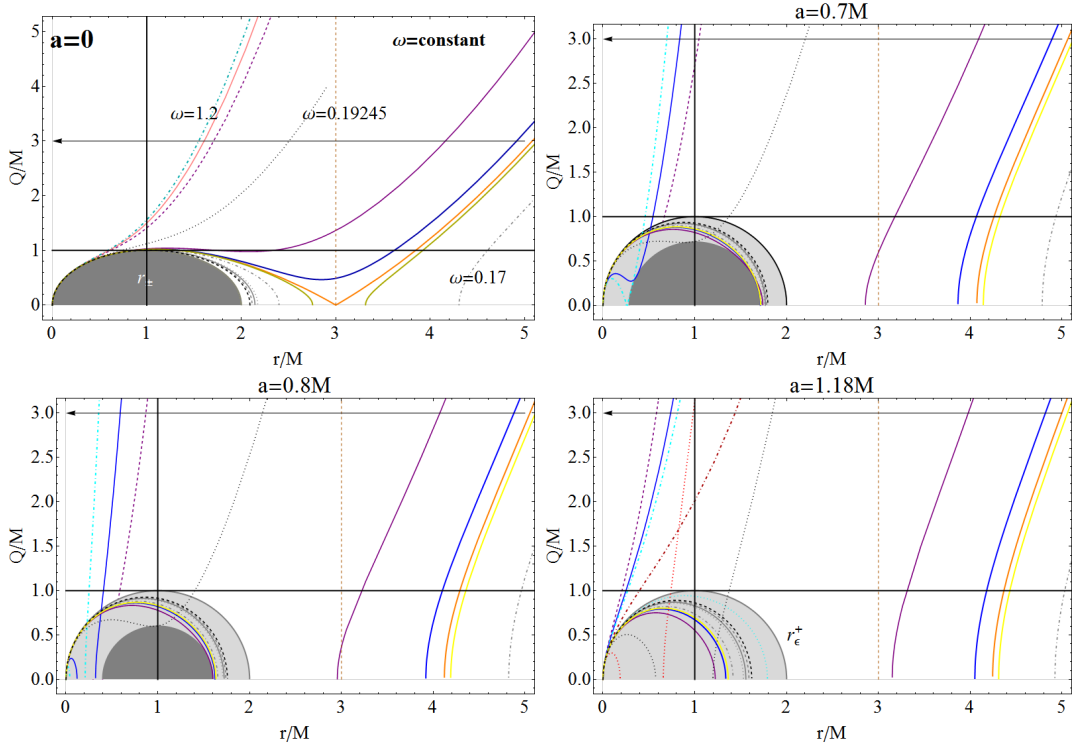


FIG. 20: Equatorial plane of the Kerr-Newman spacetimes: The surfaces $\omega_{\pm} = \text{constant}$ as functions of the radius r/M and the electrical charge Q/M —Eq. (34), for different spins. This is a generalization of the analysis shown in Fig. 8 to the case $Q \neq 0$. The black region is for $r < r_{\pm}$ and the gray region is the ergosurface Σ_{ϵ}^+ . See also Fig. 25.

Analogously to Eq. (15), we can define the functions

$$a_{\omega}^{\mp} = \frac{\mp \sqrt{r^4 \omega^2 \{ \omega^2 [Q^2 - r(r+2M)] + M^2 \} + \omega M (Q^2 - 2rM)}}{\omega^2 [Q^2 - r(r+2M)]}, \quad \text{and} \quad (34)$$

$$(Q_{\omega}^{\pm})^2 \equiv \frac{r \{ \omega^2 [a^2 (r+2M) + r^3] - 4aM^2 \omega - rM^2 + 2M^3 \}}{(a\omega - M)^2}, \quad (35)$$

where, in particular, for the **RN** static case ($a = 0$), we find

$$\text{RN:} \quad (Q_{\omega}^{\pm})^2 = r \left(\frac{r^3}{M^2} \omega^2 - r + 2M \right) \quad \text{or} \quad \omega_{\pm} = \pm \frac{M \sqrt{Q^2 + (r-2M)r}}{r^2}. \quad (36)$$

Note that while the horizons r_{\pm} can be re-parametrized for the total charge Q_T and its variation with respect to the parameter Q_T is exactly the same as for the corresponding radii r_{\pm} in the **RN** or Kerr solution, the surfaces $\omega_{\pm} = \text{constant}$ do not depend directly on Q_T ; this means that the two parameters play a different role in the solutions $\omega_{\pm} = \text{constant}$, although the envelope surfaces depend on Q_T alone. For $Q = 0$, the surfaces a_{ω}^{\pm} are shown in Fig. (30). The surfaces $\omega_{\pm} = \text{constant}$ of Eqs. (34) are shown in Figs. 20 and 25. This is a generalization of the case $Q \neq 0$ of the analysis shown in Fig. 8. Also in this case, we consider some limiting solutions to fix the different contributions of the two charge components:

$$\lim_{r \rightarrow 0} Q_{\omega}^{\pm} = 0, \quad \lim_{r \rightarrow 0} a_{\omega}^{\pm} = \frac{M}{\omega}, \quad \lim_{r \rightarrow 0} \omega_{\pm} = \frac{M}{a}. \quad (37)$$

An analysis of the spins $a_{\omega}^{\pm} = \text{constant}$ for the static limits r_{ϵ}^{\pm} on the equatorial plane is shown in Fig. 23.

Equations (37) show that in the limits considered the frequency is related to the spin source independently of the electric charge—Fig. 21. This suggests that we should define the origin of the **KN** metric bundles g_{ω}^{\pm} as dependent on the spin a/M only. It should be considered that the Killing horizons are characterized by the “rotation charge”, but ω_{H}^{\pm} does not “carry” any electric charge; that is, we can always define metric bundles considering $\omega_0 = M/a$ and the

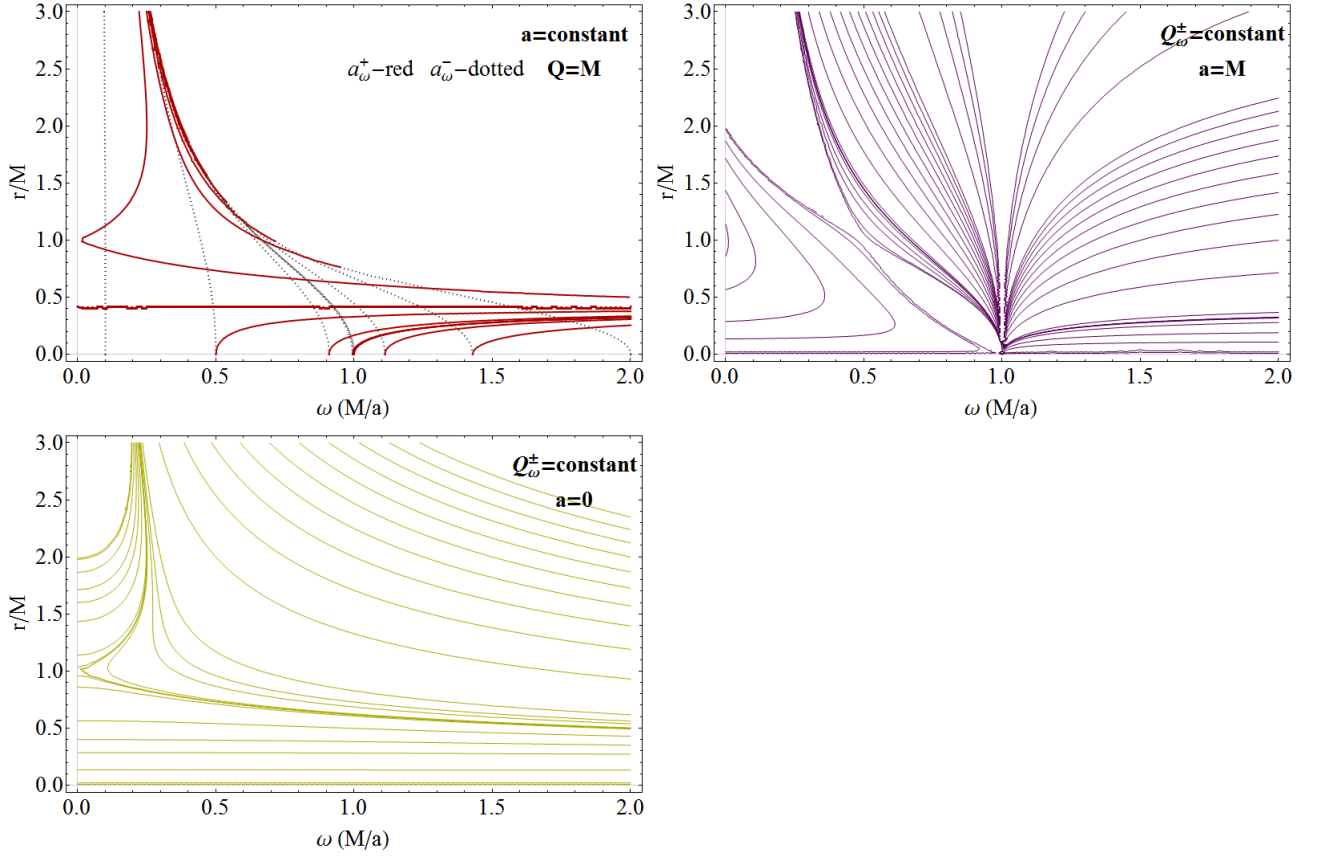


FIG. 21: Equatorial plane of the Kerr-Newman spacetimes. The frequencies $\omega_{\pm} = \text{constant}$, charge $Q_{\omega}^{\pm} = \text{constant}$, and spins $a_{\omega}^{\pm} = \text{constant}$ for some limiting cases— Eq. (37).

horizon frequencies. Explicitly, we can generalize the analysis of Sec. IV, considering a surface $a_g(a_0; Q)$ in the case $a_0 \neq 0$, where Q is a parameter, and we obtain

$$a_0 = \frac{2M^2 - Q^2 \mp 2M\sqrt{M^2 - (a^2 + Q^2)}}{a} \quad (r_{\mp}), \quad a_g^{\mp}(a_0) = \frac{a_0(2M^2 - Q^2) \mp 2M\sqrt{a_0^2(M^2 - Q^2) - Q^4}}{a_0^2 + 4M^2} \quad (38)$$

$$\text{where } a_0 > a_L(Q) \equiv \sqrt{-\frac{Q^4}{Q^2 - M^2}} \quad \text{implying } Q^2 \in]0, M^2[, \quad (39)$$

—Fig. 24. Adopting a notation analogue to the one used in Sec. IV, we solve the equation $a_{\omega}^{\pm}(r_{\pm}, \omega_0) = a$ (similarly, we could have used Q_{ω}^{\pm}) and introduce the two functions a_g^{\pm} . However, we can exploit the fact that all the curves in Figs. 20 and 25 tend to the point $(r = 0, Q = 0)$, that is, to the Kerr singularity. Approaching the static limit in the extended plane, we consider the solutions of $Q_{\omega}^{\pm}(r_{\epsilon}^{\pm}, \omega_0) = Q$:

$$Q_{\omega}^{\epsilon} \equiv \sqrt{2}\sqrt{a^2 - aa_0 + \sqrt{2M}\sqrt{a(a_0 - a)}} \quad (40)$$

as shown in Fig. 22.

We can see that in the extended plane it is necessary to consider the entire range of parameter values $(a/M, Q/M)$, including the **BH** case to describe the **NSs**. For the equatorial plane, the analysis carried out for the case $Q = 0$ is confirmed also in presence of an electric charge. For predominant spins, any curve $\omega = \text{constant}$ crosses the horizons at some points. We also see the bending of the curves limited above from the inner horizon r_- , confirming the results of Sec. IV, although with differences which are evident as the electric charge increases. The generalization of the analysis of Fig. (10) is presented in Figs. (27) and (28). We will not enter into the details of this analysis; instead, we only mention that in the **KN** case a more articulated situation for the Killing throat and bottleneck appears, when the effects of the electric charge are combined with those of the frame-dragging. The frequencies ω_{\pm} are plotted as functions of r/M for different values of the charge Q/M and spin a/M in Fig. (26). In these plots, the static and

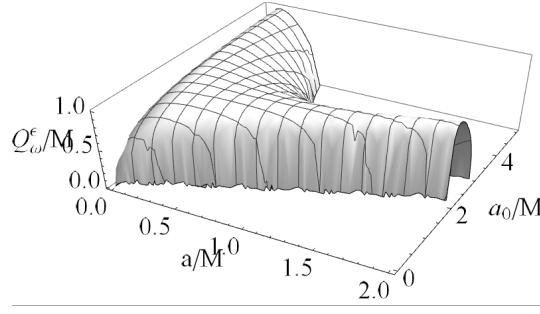


FIG. 22: Charge Q_ω^ϵ , solution of $Q_\omega^\pm(r_\epsilon^\pm, \omega_0) = Q$ defined in Eq. (40).

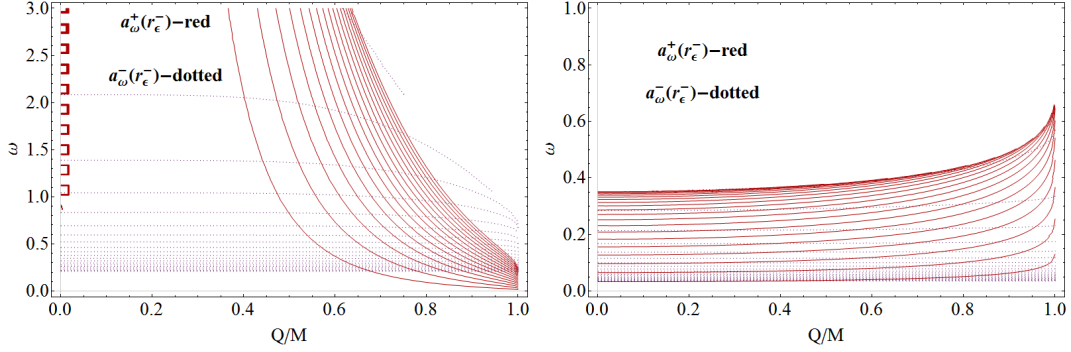


FIG. 23: Spins $a_\omega^\pm = \text{constant}$ on the static limits r_ϵ^\pm on the equatorial plane

axisymmetric cases are compared and the contribution of an electric charge are confronted with those of weak **NS** geometries. In the static geometries, the Killing throat and bottleneck still appear, while the effects of the rotation emerge as a disruption of the symmetry around the axis $\omega = 0$ of the static case and become evident in the coalescence phases of the horizons. Figures (29), (31) and (30), on the other hand, show the solutions of $\partial_r^2 \omega_\pm = 0$ and $\partial_r^3 \omega_\pm = 0$ defining the Killing bottlenecks of naked singularities, which are generalizations of the analysis presented in Fig. (5) for the case $Q = 0$ (Kerr spacetime). The surfaces $a_\omega^\pm(r, \theta)$ are shown in Fig. (30), giving a view of the solutions for the light surfaces in the off-equatorial case.

This analysis confirms the results of Secs. III and IV and the role of the frame-dragging.

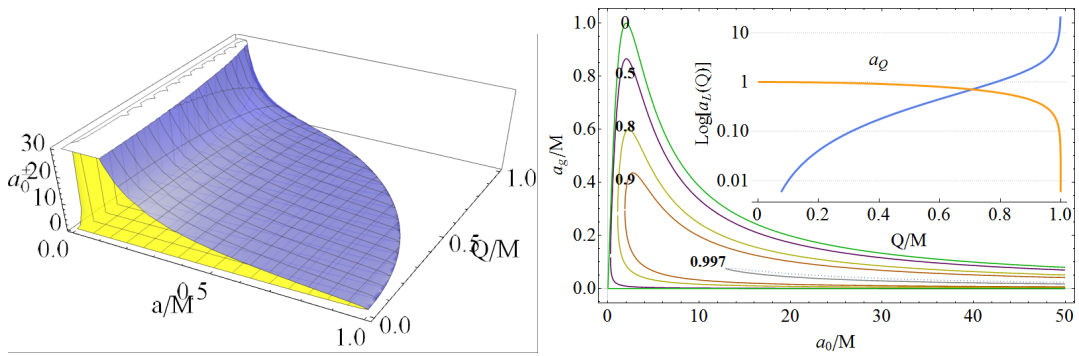


FIG. 24: *Left panel:* Three dimensional plot of a_0/M , Eq. (38), as a function of a/M and the charge Q/M . *Right panel:* Spin a_g/M as a function of a_0/M for different charge to mass ratios Q/M . *Inside panel:* Plot of $a_L(Q)$, where $a_Q \equiv \sqrt{M^2 - Q^2}$, a_g is defined for $Q \in]0, M[$ and $a_g \geq a_L(Q)$ —see Eq. (38). **BH** Killing horizons are defined by the condition $a \leq a_Q$ (for $a > 0$).

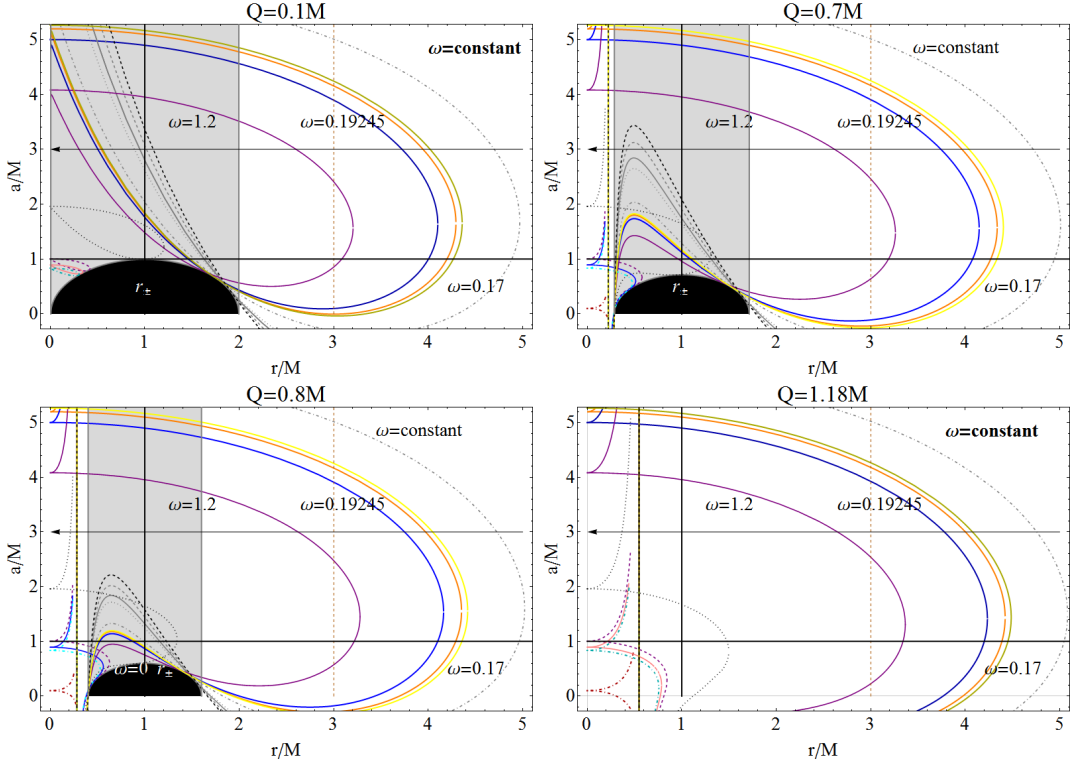


FIG. 25: Equatorial plane of Kerr-Newman spacetimes: The surfaces $\omega_{\pm} = \text{constant}$ as functions of the radius r/M and the spin a/M —Eqs (34), for different charges Q . This is a generalization to the case $Q \neq 0$ of the analysis shown in Fig. 8. The black region is for $r < r_{\pm}$ and the gray region represents the ergosurface Σ_{ϵ}^{+} . See also Fig. 20.

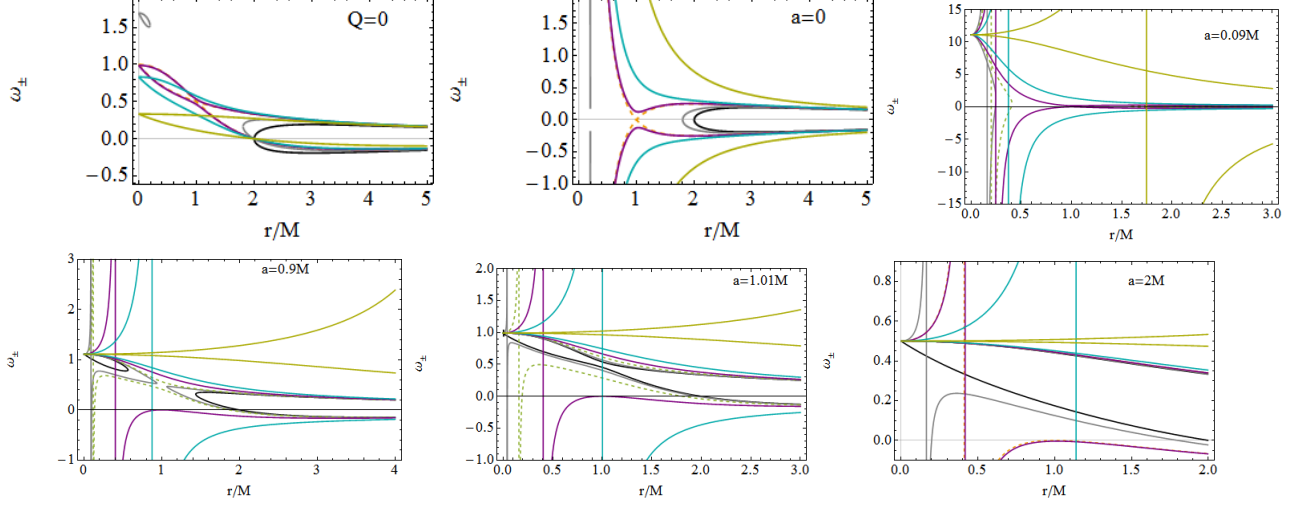


FIG. 26: Equatorial plane of the Kerr-Newman spacetime: The frequencies ω_{\pm} given in Eq. (34) as functions of r/M for different values of the charge Q/M and spin a/M . The limiting cases of the Kerr spacetime ($Q = 0$) is shown in the first upper left panel and the static Reissner-Nordström geometry with $a = 0$ is the second left upper panel. The analysis shows the emergence of coalescence of the Killing horizons r_+ and r_- in the extreme black hole geometries and the emergence of a Killing throat and Killing bottleneck in the NS geometries—see also Figs. (2,1,11,27 and 28).

VI. CONCLUDING REMARKS AND FUTURE PERSPECTIVES

In this work, specially in Sec. III, we explored the Killing throats and bottlenecks, arising from the properties of stationary observers in the Kerr geometries. In the case of **WNSs** ($a/M \in [1, 2]$), the Killing throats show “restrictions”,

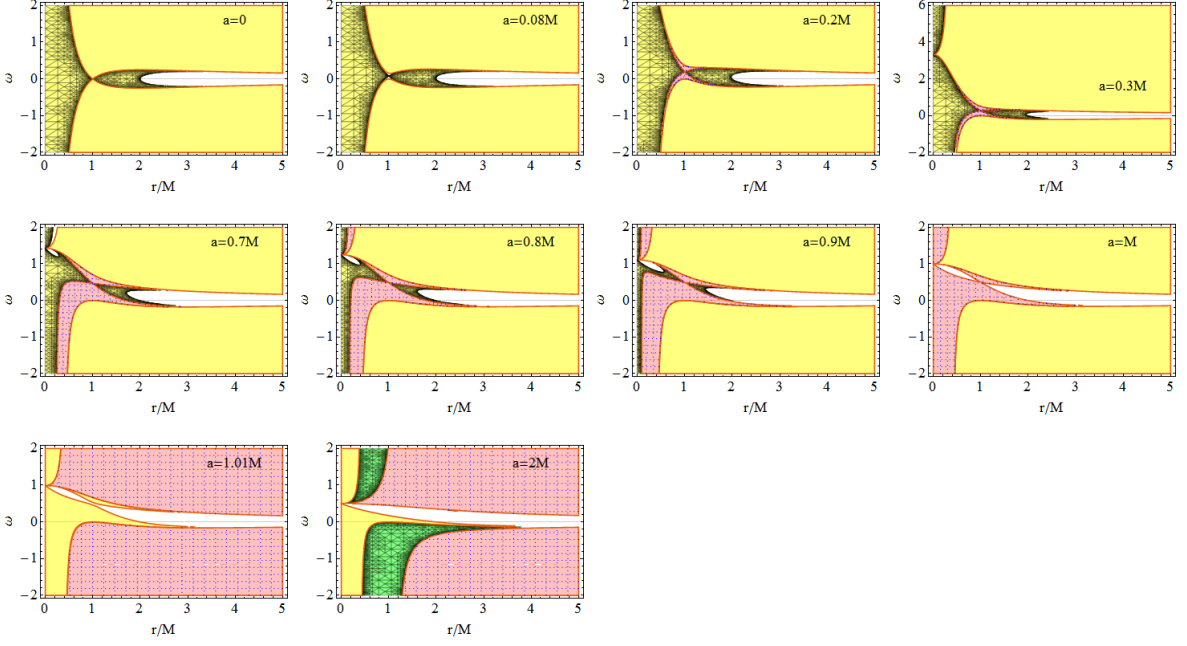


FIG. 27: Equatorial plane of the Reissner-Nordström spacetime: generalization of the analysis of Fig. 10 and 28 for the case $a = 0$ and $Q \neq 0$.

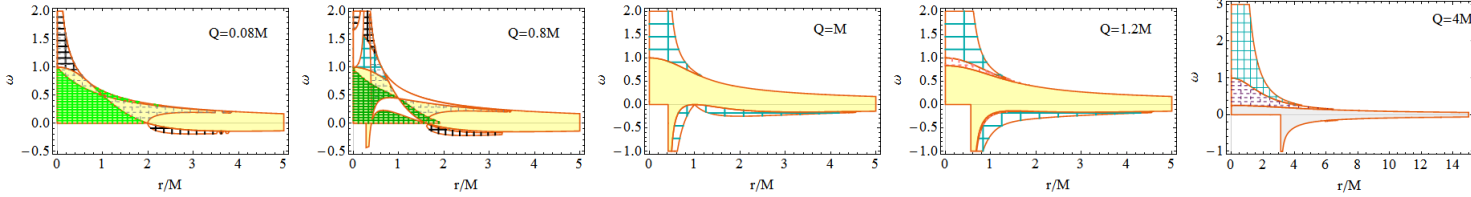


FIG. 28: Equatorial plane of the Kerr-Newman spacetime: generalization of the analysis of Fig. 10 to the case $Q \neq 0$ —see also Fig. 27

which we identify as Killing bottlenecks. To explore the properties of the bottlenecks, we introduced in Sec. (IV) the concept of extended plane, which is a graph relating a particular characteristic of a spacetime in terms of the parameters entering the corresponding spacetime metrics. More precisely, the analysis of some peculiar characteristics of the bottlenecks, defined as horizons remnants, indicated some links between **BHs** and **NSs** (and in particular **WNSs**). To compare the **BH** and **NS** characteristics, it was convenient to introduce in Sec. IV the concept of metric bundles, i.e., curves in the extended plane π_a^+ , representing a collection of metrics defined by a particular photon orbital frequency, named metric bundle frequency. The bundle frequencies (and the orbital limiting frequencies in any point on the equatorial plane of any spacetime of the family) are all and only the frequencies of the horizon defined in the extended plane. This analysis has been done mainly on the equatorial plane of axisymmetric geometries. Metric bundles show, in fact, the remarkable property to be tangent to the horizon curve in the extended plane, the space where the curves representing the metric bundles are defined. In the case of the the equatorial plane of the Kerr metric, the extended plane is essentially equivalent to the function that relates the frequency with the spin. Notably, the metric bundle associated to the extreme Kerr **BH** corresponds to a regular curve tangent to the horizon with bundle origin $a_0 = 2M$. As proved in Sec. IV, *all* the metric bundles are tangent to the horizon in the extended plane π_a^+ and the horizon emerges as the envelope surface of the metric bundles in π_a^+ . A bundle frequency corresponds to one limiting photon orbital frequency for all **BHs** or some **BHs** and **NSs** geometries. The bundle frequency coincides with the frequency at the (inner or outer) horizon curve, which is tangent to the metric bundle. On the other hand, the metric bundles are all defined by all and only the frequency of the horizon in π_a^+ . Viceversa, all the horizon frequencies in the extended plane are metric bundle frequencies. In Sec. V, we consider the static and electrically charged Reissner-Nordström spacetime and the Kerr-Newman axisymmetric electrovacuum solution and show that the bending (closing) of the curves of the metric bundles is due to the rotation of the gravitational source. Therefore,

we can say that the horizons frequencies determine the **BHs and NSs** limiting photon orbital frequencies. This fact establishes a connection between **BHs** and **NSs**: the inner **BH** horizon is connected to **BH** and **WNS** origin bundles, whereas the outer horizon sets the **BHs-SNSs** correspondence. In the extended plane, **NSs** are associated with portions of the horizon. In this sense, the inner horizon is partially constructed by **BH** metric bundles. The inner horizon is associated with **WNS** origins. This last property turns out to be related to the Killing bottlenecks appearing in the light surfaces. Interestingly, the outer horizon in π_a^+ is generated by **SNSs** metric bundles only. This fact has the interesting consequence that only the horizon frequencies determine the frequencies ω_{\pm} at each point, r , on the equatorial plane of a Kerr **BH** or **NS** geometry: all the frequencies $\omega_{\pm}(r)$ on the equatorial plane are only those of the horizon in π_a^+ , the horizon in π_a^+ contains information about all limiting photon orbits also in **NS** spacetimes. In Secs. III and IV, we have also introduced the concept of inner horizon confinement. In this sense, **NSs** are “necessary” for the construction of horizons. The outer horizon is associated with a **NS** (the bundle origin) in the extended plane and the inner horizon to a **WNS** or a **BH**. Therefore, we believe that this result could be of interest for the investigation of gravitational collapses in which connections between **NS** and **BH** solutions are expected and emerge [55–57].

Some further aspects of these properties are currently under investigation. Firstly, it would be necessary to further analyze the off-equatorial case and test the results of Sec. IV in other kinds of geometries. In a future analysis, we shall analyze other axisymmetric spacetimes admitting Killing horizons and consider the possible thermodynamic implications of the results discussed here, particularly, in relation to the possibility of formulating the **BH** thermodynamic laws in terms of metric bundles. We also point out that metric bundles and horizons remnants seem to be related to the concept of pre-horizon regimes. There is a pre-horizon regime in the spacetime when there are mechanical effects allowing circular orbit observers, which can recognize the close presence of an event horizon. This concept was introduced in [1] and detailed for the Kerr geometry in [58, 59]. The pre-horizon was identified and analyzed in [2], leading to the conclusion that a gyroscope would observe a memory of the static case in Kerr metric. Clearly, this aspect could be of relevance during the gravitational collapse [23, 60–62].

We now summarize the main aspects of our analysis focusing on the possible interpretation of the main results.

(i) We identified bottlenecks essentially as *horizon remnants*. Similar interpretations have been presented in [1, 2, 58, 59], by using the concept of pre-horizons, and in [34], by analyzing the so-called whale diagrams. These structures could play an important role for describing the formation of black holes and for testing the possible existence of naked singularities. Notably, the concept of remnants, as expressed here, refers to and evokes a sort of spacetime “plasticity”, which naturally led to the introduction in Sec. (IV) of the concept of the extended plane. In this new frame, we found several properties emerging from and affecting the spacetime geometries when we consider an entire family of solutions as a *unique geometric object*.

(ii) Considering the Kerr family as a single object, the geometric quantities (for example, the horizons) defined for a single solution acquire a completely different significance when considered for the entire family.

(iii) Considering metric bundles with **WNS**, we found that the inner horizon is confined in the metric bundle framework.

(iv) We proved the existence of a connection between black holes and naked singularities. To each **BH** corresponds the pair (**WNS**, **SNS**) or the pair (**BH**, **SNS**). This correspondence is important for the definition of the Killing horizons.

(v) We proved that **WNSs (SNSs)** are necessary for the construction of the inner (outer) Killing horizon. This result could shed light on the physical meaning of **NSs** solutions.

To conclude, we present a schematic summary of the main results presented in this work.

- Analysis of *Killing throats* and definition *Killing bottlenecks* for particular naked singularities—Section III. To define Killing throats, we study the limiting photons surfaces r_{\pm}^{\pm} and frequencies ω_{\pm} which are defined in Eq. (11) and Eq. (8), respectively. We also interpret bottlenecks as *horizons remnants* in weak naked singularities.
- *Inner horizon confinement*—Sec. III. In Eq. (13), we identify the photon orbits characterized by the horizons orbital frequencies. The radii r_{\pm}^{\mp} represent the set of photon orbits with frequencies ω_{\pm}^{\mp} at the **BH** horizons—Eq. (13)—Fig. 1. The inner horizon confinement, according to the constraints on r_{-} , is in agreement with the confinement of the metric bundles containing **BHs** and **WNSs** (see Sec. IV).
- Definition of the *extended plane* π_a and *metric bundles* g_{ω} in Sec. IV. Metric bundles are curves in π_a tangent to the horizons characterized by the limiting photon frequency ω_{+} or ω_{-} .
- *Tangency condition and horizon construction in the extended plane*. We demonstrate that the horizon curve corresponds to the envelope surface of the metric bundles. All the metric bundles are tangent to the horizon curve and all the points of the horizons are associated to one and only one metric bundle tangent to that point— Figs. 14, 15, 16 and Tables III and II. Consequently, all the limiting photon orbital frequencies (on the

equatorial plane) are **all and only** the frequencies of the horizon curve in π_a , related to two metric bundles, with frequencies ω_0 and ϖ_{\pm} , respectively. Particularly, through the relationship between metric bundles and horizons in π_a^+ , a **NS** or **BH** metric can be parameterized in terms of the horizon frequency identified by the corresponding metric bundle. The inner and outer horizons in π_a^+ correspond to envelope surfaces. We analyze the lines $a = \text{constant}$ (i.e. a single spacetime of the metric bundle) and $r = \text{constant}$ in the extended plane—Fig. 8 and classify the singularities according to the horizon construction as shown in Fig. (13), i.e., strong naked singularities, **SNS** = **SNS**⁺ \cup **SNS**[−], having $a_0 > 2M$ with **SNS**⁺ for $a_0 > 4M$ and **SNS**[−] for $a_0 \in [2M, 4M[$; **WNS**—weak naked singularities with $a_0 \in]M, 2M[$ and **BH** = **BH**⁺ \cup **BH**[−] with **BH**⁺ for $a \in [a_g^1, M]$, $a_g^1 = 3/4M$ and **BH**[−] for $a \in [0, a_{g_1}]$.

- Demonstration of the *confinement* of metric bundles with origin in **BHs** and **WNSs** and identification and study of the *corresponding bundles*. In Table II, we proved the confinement of the bundles in the extended plane delimited by the inner horizon curve. The horizon and bundle frequencies are related by the relation $\omega_0^+ \omega_0^- = 1/4$.
- *Properties of horizons and bundles*. For the entire family of Kerr geometries, we established the relations between metric bundles and horizons. We found two relations which can be specified in detail as follows. Relations **I**: $\omega_0^{-1} \equiv a_0^{\pm}/M = (2r_{\pm}(a_g)/a_g) \equiv \omega_H^{-1}(a_g)$, $\omega_H^+(r_g, a_g) = \omega_0 = Ma_0^{-1}$, $\omega_H^-(r'_g, a_g) = \omega'_0 = M/a'_0$ where $r'_g \in r_-(r_+ = r_g, r_- = r'_g)$ —Fig. (13). Relation **II**: $\omega'_0 = (4\omega_0)^{-1}$, $\omega_H^+ \omega_H^- = 1/4$, (or equivalently $a_0^+(a_g)a_0^-(a_g) = 4M^2$), $a_0^{\pm}/M = (2r_{\pm}(a_g))/a_g$ where $a = a_0$ and $a = a_p$ —Fig. 14.
- Properties of specific spacetimes. We studied the metric bundles corresponding to a single **BH** spacetime (with equal tangent spin a_g). We analyzed the Kerr spacetime in terms of metric bundles—Sec. IV.
- Proof of the **BH-NS** relation through the properties of the corresponding metric bundles.
- Analysis of the frequencies ϖ_{\pm} of the spacetime by using the maximum crossing of two metric bundles—Eq. (22). We proved the existence of the corresponding metric bundles and analyzed its significance for the horizon construction and properties of a **BH** spacetime—Tables II and III; Figs. 13,14,15,15,16,17 and Eqs. (19) and (27).
- Identification of the Killing throats and bottlenecks and metric bundles in the static and charged *Reissner Nordström* solution and in the axisymmetric, electrically charged, *Kerr-Neumann spacetime*. We proved that the bending (curvature) of the Kerr metric bundles in π_a is related to the frame-dragging of the spinning spacetimes. We noticed the different roles played by the electric and rotational charges—Eq. (28). We studied the metric bundles $(Q_{\omega}^{\pm})^2$ in terms of the electric charge Q —Eq. (35). In Sec. A, we analyzed the off-equatorial case of the Kerr and Kerr-Newman geometries. In Sec. B, we considered the relations between the areas of the horizon and of the metric bundles regions in the extended plane.

Acknowledgments

D.P. acknowledges partial support from the Junior GACR grant of the Czech Science Foundation No:16-03564Y. D.P. is grateful to Donato Bini, Fernando de Felice and Andrea Geralico for discussing many aspects of this work. This work was partially supported by UNAM-DGAPA-PAPIIT, Grant No. 111617, and by the Ministry of Education and Science of RK, Grant No. BR05236322 and AP05133630.

Appendix A: Analysis of the Kerr and Kerr-Newman geometries: the off-equatorial case

In this appendix, we summarize the analysis presented in Secs. III, IV and V for off-equatorial stationary observers in Kerr and Kerr-Newman spacetimes. We focus on the presentation of the corresponding plots which contain all the relevant information for this case.

Appendix B: Areas of the horizon and of the metric bundles regions in π_a^+

In this section, we analyze the area of the regions of π_a^+ in Fig. 8 bounded by the curves a_{ω}^{\pm} for $\omega = \text{constant}$, between \mathcal{P}_S and \mathcal{P}_L , including the entire collection of spacetimes $\mathbf{g} \in]g_{\omega}^-, g_{\omega}^+[$ bounded by $(g_{\omega}^-, g_{\omega}^+)$. We compare this region with the (inaccessible) section in π_a^+ bounded by the horizons r_{\pm} .

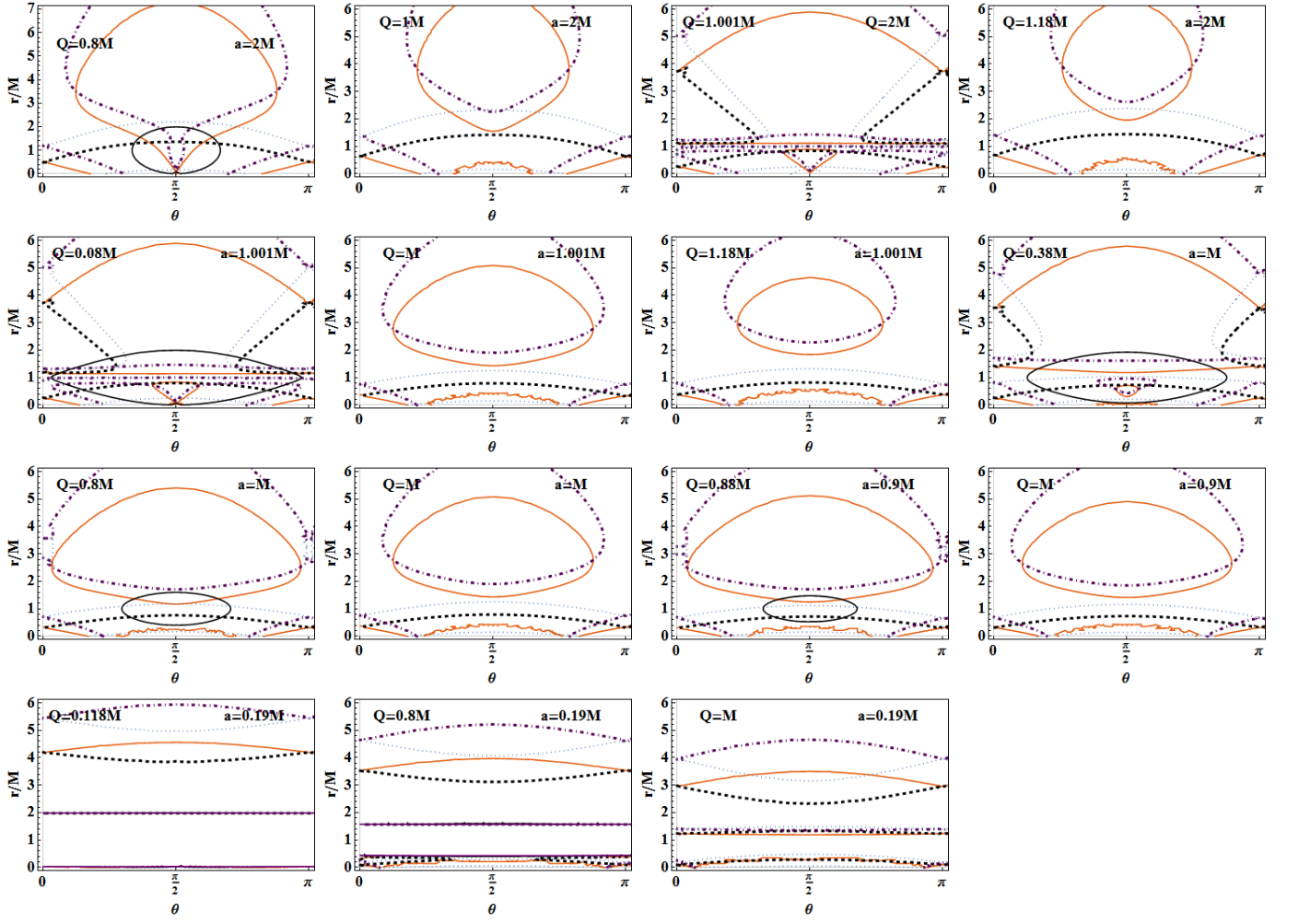


FIG. 29: Kerr-Newman spacetimes: Off-equatorial analysis. Solutions of $\partial_r^2 \omega_{\pm} = 0$ (orange and dashed curves) and $\partial_r^3 \omega_{\pm} = 0$ (dotted and dotted-dashed curves), defining the Killing bottleneck of naked singularities. Solutions of $g_{tt} = 0$ (black), defining the static limits, and $g_{rr}^{-1} = 0$ (red) defining the horizons. See also Fig. (31) for the case $Q = 0$ (Kerr spacetimes).

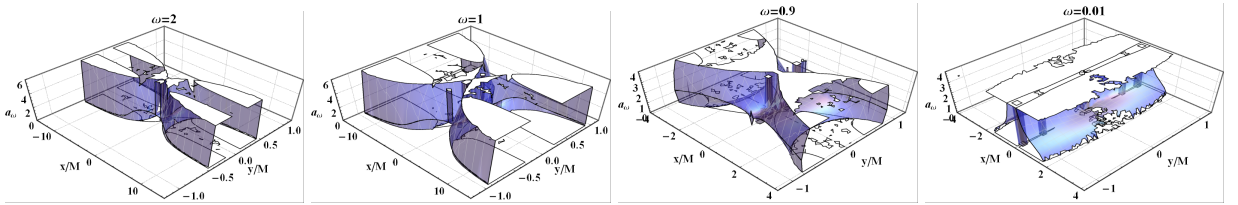


FIG. 30: Kerr spacetimes: Off-equatorial analysis. The surfaces $a_{\omega}^{\pm}(r, \theta)$ as functions of the radial distance r in Cartesian coordinates (x, y) for different frequencies values ω , including **BHs** and **NSs**—see also Figs. 31, 27 and 28. The spin functions are in Eq. (33) for $Q = 0$.

First, note that each region bounded by g_{ω}^{\pm} can be decomposed into other non-disjoint metric bundles. In fact, as can be seen in Fig. 8, the metric bundles g_{ω}^{\pm} cross each other in π_a^+ . This corresponds to the fact that for a fixed point $p = (a/M, r/M) \in \pi_a^+$, different frequencies are possible, i.e., a light-like particle can have different orbital frequencies corresponding to the two solutions ω_{\pm} . To explore this aspect and also the **BH-NS** connection, we introduce the radii

$$r_{\beta}/M \equiv \frac{2}{4\omega^2 + 1}, \quad r_{\nu}/M \equiv \frac{1 - \omega}{\omega}, \quad r_{\pi}/M \equiv \frac{\sqrt{\frac{1}{\omega^2} + \frac{6}{\omega} - 7\omega + \omega - 1}}{2\omega}, \quad (\text{B1})$$

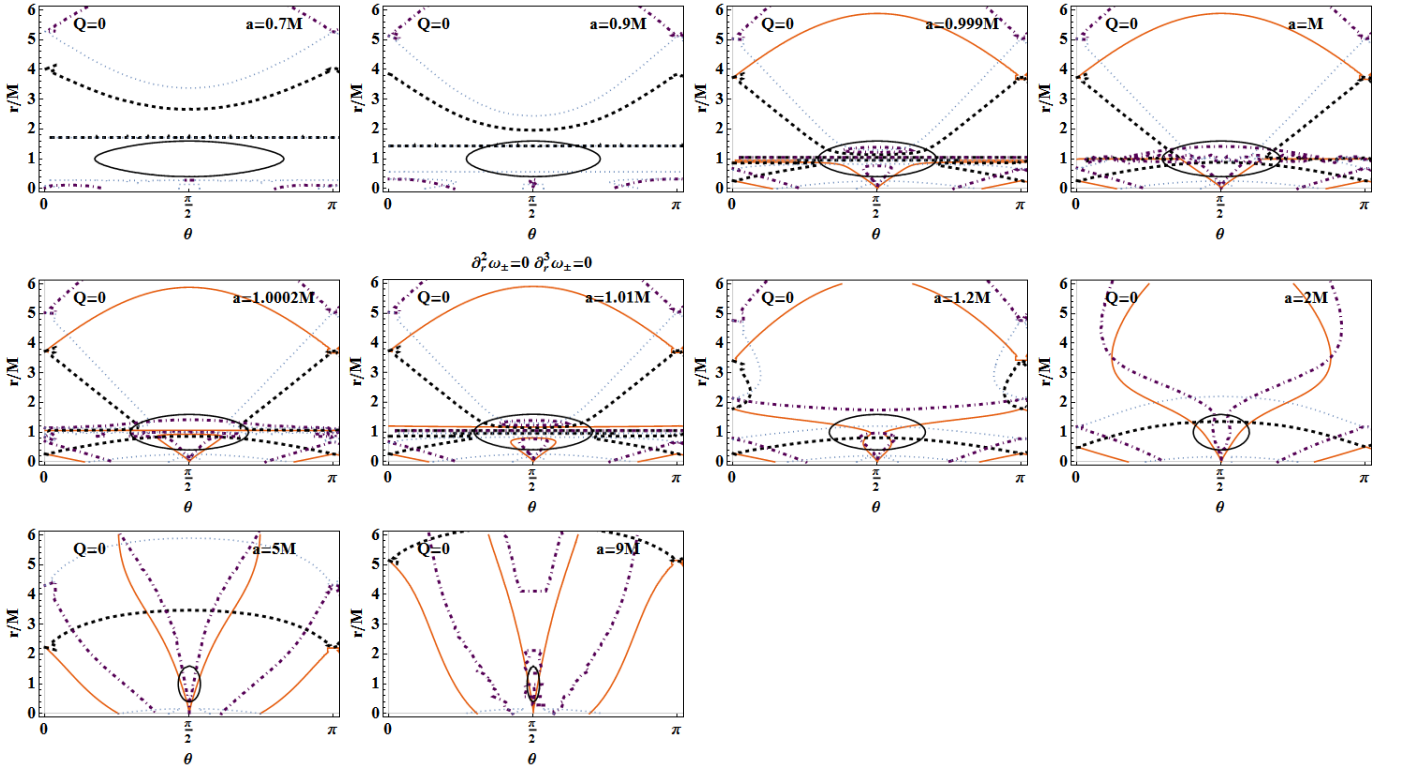


FIG. 31: Kerr geometries: Off-equatorial case. Solutions of $\partial_r^2 \omega_{\pm} = 0$ (orange and dashed curves) and $\partial_r^3 \omega_{\pm} = 0$ (dotted and dotted-dashed curves), defining the Killing bottlenecks of naked singularities, $g_{tt} = 0$ (black), defining the static limits, and $g_{rr}^{-1} = 0$ (red), defining the horizons. See also Fig. (29) for the case $Q = 0$ (Kerr spacetimes).

which are plotted in Fig. 11 as functions of the frequency ω . It is clear that the functions $\{r_{\beta}, r_{\nu}, r_{\pi}\}$ are limiting radii. A generalization of this study is also discussed in Sec. V, where we consider the Reissner-Nordström and Kerr-Newman geometries.

The areas \mathcal{A} correspond to the regions of the extended plane π_a^+ bounded by a_{ω}^{\pm} and are confronted here with the areas of the region bounded by the horizons $\mathcal{A}_{r_{\pm}^+} = \pi/2$. An analysis of these areas is shown in Figs. 32. We can write the areas \mathcal{A} as functions of the frequency ω of the metric bundles g_{ω}^{\pm} or, equivalently, the spin origins $a_0 = M/\omega$, as follows

$$\mathcal{A}(\omega) = |f_{\mathcal{A}}(r, \omega)|_{r_{\partial^+}} - f_{\mathcal{A}}(r, \omega)|_0|, \quad (\text{B2})$$

$$f_{\mathcal{A}}(r) \equiv \frac{\omega [c_1 \omega + 4 \log [(r+2)\omega^2 + \Omega + 1] + (r-3)\Omega] + i(1-3\omega^2) \log(2[\Omega - i(r+1)\omega]) - 4\omega \log(r+2)}{\omega^2},$$

$$\mathcal{A} = \frac{1}{\omega^2} [3\omega - 4\omega \log(r_{\partial^+}^+ + 2) + i(3\omega^2 - 1) \log(2 - 2i\omega) + i \log(-2ir_{\partial^+}^+) + \omega \{-3i\omega \log(-2ir_{\partial^+}^+) - 4 \log(\omega^2 + 1) + 4 \log[(r_{\partial^+}^+ + 2)\omega^2 + 1]\}], \quad (\text{B3})$$

where dimensionless quantities $r \rightarrow r/M$ have been used. We also define the quantities $\bar{\mathcal{A}}(\omega) \equiv f_{\mathcal{A}}(r)|_{c_1=0}$ and $\Omega \equiv \sqrt{1 - r(r+2)\omega^2}$, where $f_{\mathcal{A}}(r, \omega)$ is a function of the frequency $\omega = M/a_0$ of the metric bundle and of the radius r . Moreover, c_1 is an integration constant. From Fig. 32, it is clear that the area \mathcal{A} is a decreasing function of the frequency ω , which is in agreement with the results of Fig. 8. Indeed, the metric bundles shrink at the origins $a_0 < M$, that is, for frequencies $\omega_0 = M/a > M$, where g_{ω}^{\pm} are all contained in $r \in [0, r_-]$. Viceversa, the area grows as the spin-mass ratio of the **NS** increases. The right panel of Fig. 32 shows an area $\mathcal{A} = \text{constant}$ with respect to the frequency ω and the radius r/M . Special cases correspond to the limiting geometries \mathcal{P}_{\odot} and \mathcal{P}_{\otimes} . Finally, the evaluation of the areas in π_a^+ takes into account the curvature of the curves in the plane. Therefore, it is necessary to consider some relative quantities reported below and represented in Fig. (32). Considering the quantities

$$\Delta^{\pm} a_{\omega} \equiv a_{\omega}^+ \pm a_{\omega}^-; \quad \text{where} \quad \Delta^+ a_{\omega} = \frac{4M}{(r+2M)\omega}, \quad \Delta^- a_{\omega} = \frac{2\sqrt{r^2\omega^2 [M^2 - r(r+2M)\omega^2]}}{(r+2M)\omega^2 M}, \quad (\text{B4})$$

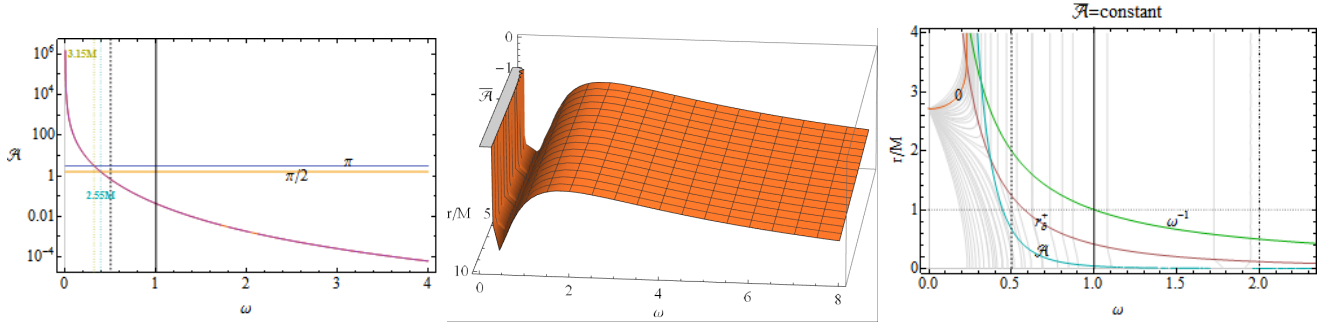


FIG. 32: The areas \mathcal{A} of the regions of the extended plane π_a bounded by a_ω^\pm of Fig. 8. The areas \mathcal{A} , $\bar{\mathcal{A}}$ and $\mathcal{A}_{r_\pm} = \pi/2$ of the region bounded by the horizons r_\pm in π_a^+ -region $a \gg 0$ - $\mathcal{A}_{r_\pm}^+$ are defined in Eq. (B2). Left panel: Area \mathcal{A} as a function of the frequency ω . The areas \mathcal{A}_{r_\pm} and $2\mathcal{A}_{r_\pm}$ are also shown. Frequencies corresponding to solutions $\mathcal{A}_{r_\pm} = \mathcal{A}$ and $2\mathcal{A}_{r_\pm} = \mathcal{A}$ are pointed with vertical lines. The corresponding geometries ($a = M/\omega$) are shown. Center panel: Area \mathcal{A} as a function of the frequency ω and radius r/M . The role of the frequencies $\omega = 2$ and $\omega = 0.5$ is indicated. Right panel: Curves $\mathcal{A} = \text{constant}$ as functions of the frequency ω and radius r/M . The curves $\mathcal{A} = 0$ are red colored. The area \mathcal{A} , radius r_\pm^+ and ω^{-1} are also plotted. Negative areas correspond to solutions $a < 0$. See also Fig. 9 for a 3D representation of these regions.

and using r_\pm^+ in Eq. (16), we can obtain the area \mathcal{A} of the regions bounded by the curves a_ω^\pm , between the points \mathcal{P}_S and \mathcal{P}_C . The curves bending the area \mathcal{A} are related to solutions of the equation $\partial_\omega^2 \Delta^- a_\omega = 0$, which is solved for $r/M = \sqrt{(3\omega^2 + 2)/\omega^2}/(\sqrt{3} - 1)$, while the only solutions $\partial_{r/M}^2 \Delta^- a_\omega = 0$ are for the frequencies $\omega = \sqrt{2}M^2/(\sqrt{r(r+2M)}(r+3M)M)$ in the frequency range $\omega \in]0, 1.78015[$, where the distance between the two curves is extreme. These quantities, considering the variation of $\Delta^- a_\omega$ with respect to the frequencies and the radius r respectively, are related to the curvature of the $\Delta^- a_\omega$, where the extreme radius as function of the frequency ω is

$$\frac{r_{\Delta_\omega^+}^1}{M} = \frac{1}{3} \left(\sqrt[3]{\frac{27}{\omega^2} + 3\sqrt{\frac{81}{\omega^4} + \frac{60}{\omega^2} - 27 + 10}} + \sqrt[3]{\frac{27}{\omega^2} - 3\sqrt{\frac{81}{\omega^4} + \frac{60}{\omega^2} - 27 + 10} - 5} \right) \quad \omega \in [0, 1.178] \quad (\text{B5})$$

$$\frac{r_{\Delta_\omega^+}^2}{M} = \frac{1}{3} \left(2\sqrt{7} \cos \left[\frac{1}{3} \cos^{-1} \left(\frac{10\omega^2 + 27}{7\sqrt{7}\omega^2} \right) \right] - 5 \right), \quad \omega > 1.178. \quad (\text{B6})$$

-
- [1] F. de Felice, *Mont. Notice R. astr. Soc.* **252**, 197-202, (1991).
 - [2] F. de Felice and S. Usseglio-Tomasset, *Class. Quantum Grav.* **8**, 1871-1880 (1991).
 - [3] P. T. Chrusciel, J. Lopes Costa and M. Heusler, *Living Rev. Rel.* **15**, 7 (2012).
 - [4] R. M. Wald, *Class. Quant. Grav.* **16**, A177 (1999).
 - [5] R. M. Wald, *Living Rev. Relativ.* **4**(1), 6 (2001).
 - [6] Z. Li and C. Bambi, *Phys. Rev. D* **87**, 124022 (2013).
 - [7] T. Jacobson and T. P. Sotiriou, *J. Phys. Conf. Ser.* **222**, 012041 (2010).
 - [8] S. L. Shapiro and S. A. Teukolsky, *Phys. Rev. Lett.* **66**, 994 (1991).
 - [9] R. Goswami, P. S. Joshi and P. Singh, *Phys. Rev. Lett.* **96**, 031302 (2006).
 - [10] J. P. S. Lemos, G. M. Quinta and O. B. Zaslavskii, *Phys. Rev. D* **93**, no. 8, 084008 (2016)
 - [11] D. Pugliese, H. Quevedo and R. Ruffini, *in Proceedings, 12th Marcel Grossmann Meeting on General Relativity, Paris, France, July 12-18, 2009. Vol. 1-3,* p.1017-1021, edited: T. Damour, R. T. Jantzen and R. Ruffini, Singapore, Singapore: World Scientific (2012).
 - [12] D. Pugliese, H. Quevedo and R. Ruffini, *Phys. Rev. D* **84**, 044030 (2011).
 - [13] D. Pugliese, H. Quevedo and R. Ruffini, *Phys. Rev. D* **83**, 024021 (2011).
 - [14] D. Pugliese, H. Quevedo and R. Ruffini, *Phys. Rev. D* **83**, 104052 (2011).
 - [15] D. Pugliese, H. Quevedo and R. Ruffini, *Phys. Rev. D* **88**, 024042 (2013).
 - [16] D. Pugliese and H. Quevedo, *Eur. Phys. J. C* **75**, 5, 234 (2015).
 - [17] D. Pugliese, H. Quevedo and R. Ruffini, *Eur. Phys. J. C* **77**, 4, 206 (2017).
 - [18] D. Pugliese and H. Quevedo, *Eur. Phys. J. C* **78**, 1, 69, (2018).
 - [19] C.J.S. Clarke, F. De Felice, *Gen. Rel. Grav.*, **16**, 2, 139-148 (1984).
 - [20] D. Bini, F. de Felice, *Gen. Rel. Grav.*, **47**, 131, 11, (2015).
 - [21] F. de Felice, *A&A*, **34**, 15 (1974).
 - [22] F. de Felice, *Nature* **273**, 429-431 (1978).

- [23] C. Chakraborty, M. Patil, P. Kocherlakota, *et al.*, Phys. Rev. D **95**, 8, 084024 (2017).
- [24] M. Blaschke, Z. Stuchlík, Phys. Rev. D **94**, 8, 086006 (2016).
- [25] M. Bejger, T. Piran, M. Abramowicz and F. Hakanson, Phys. Rev. Lett. **109**, 121101 (2012).
- [26] Z. Stuchlik, P. Slany, G. Torok and M. A. Abramowicz, Phys. Rev. D **71**, 024037 (2005).
- [27] Z. Stuchlik and J. Schee, Class. Quant. Grav. **29**, 065002 (2012).
- [28] K. i. Nakao, P. S. Joshi, J. Q. Guo, *et al.* Phys. Lett. B **780**, 410 (2018).
- [29] S. Gao and Y. Zhang, Phys. Rev. D **87**, 4 044028 (2013).
- [30] Z. Stuchlik, Bull. Astron. Inst. Czech. **32**, 68 (1981).
- [31] P. Pradhan and P. Majumdar, Eur. Phys. J. C **73**, 6 2470 (2013).
- [32] M. Kolos and Z. Stuchlík, Phys. Rev. D **88** 065004, (2013).
- [33] Z. Stuchlik and J. Schee, Class. Quant. Grav. **27**, 215017 (2010).
- [34] I. V. Tanatarov and O. B. Zaslavskii, Gen. Rel. Grav. **49**, no.9, 119 (2017).
- [35] S. Mukherjee and R. K. Nayak, Astrophys. Space Sci. **363** no.8, 163 (2018).
- [36] O. B. Zaslavskii, Phys. Rev. D **98**, no.10, 104030 (2018).
- [37] E. Barausse, V. Cardoso, and G. Khanna, Phys. Rev. Lett. **105**, 261102 (2010).
- [38] P. S. Joshi, *Gravitational Collapse and Spacetime Singularities*, Cambridge Monographs on Mathematical Physics, New York (2007).
- [39] B. Giacomazzo, L. Rezzolla and N. Stergioulas, Phys. Rev. D **84**, 024022 (2011).
- [40] A. Helou, I. Musco and J. C. Miller, Class. Quant. Grav. **34**, 13, 135012 (2017).
- [41] R. M. Wald and V. Iyer, Phys. Rev. D **44**, 3719 (1991).
- [42] J. Gariel, N. O. Santos and J. Silk, Phys. Rev. D **90**, 063505 (2014).
- [43] N. Pelavas, N. Neary and K. Lake, Class. Quant. Grav. **18**, 1319 (2001).
- [44] C. Herdeiro and E. Radu, Phys. Rev. D **89**, 1240 18 (2014).
- [45] V. Cardoso, P. Pani, M. Cadoni and M. Cavaglia, Phys. Rev. D **77**, 124 044 (2008).
- [46] N. Comins and B. F. Schutz, Proc. R. Soc. A **364**, 1717 211-226 (1978).
- [47] A. V. Frolov and V. P. Frolov, Phys. Rev. D **90**, 12, 124010, (2014).
- [48] Z. Stuchlik, Bull. Astron. Inst. Czech **31**, 129 (1980).
- [49] Z. Stuchlik, J. Schee, Class. Quant. Grav. **30**, 7, 075012 (2013).
- [50] J. Schee and Z. Stuchlik, JCAP **1304**, 005 (2013).
- [51] G. Torok and Z. Stuchlik, Astron. Astrophys. **437**, 775 (2005).
- [52] J. Biák, Z. Stuchlik, and V. Balek, Bull. Astron. Inst. Czech **40**, 2 65–92 (1989).
- [53] M. Patil and P. S. Joshi, Class. Quant. Grav. **28**, 235012 (2011).
- [54] O. B. Zaslavskii, Gen. Rel. Grav. **48**, 10, 132 (2016).
- [55] R. Goswami and P. S. Joshi, Phys. Rev. D **76** 084026 (2007).
- [56] T. Crisford and J. E. Santos Phys. Rev. Lett. **118**, 181101 (2017).
- [57] V. S. Manko and E. Ruiz, arXiv:1803.03301 [gr-qc] (2018).
- [58] F. de Felice, Class. Quantum Grav. **11**, 1283-1292 (1994).
- [59] F. de Felice and S. Usseglio-Tomasset, Gen. Rel. Grav. **28**, 2 (1996).
- [60] F. de Felice and S. Usseglio-Tomasset, Gen. Rel. Grav. **24**, 10 (1992).
- [61] F. de Felice and L. Di G. Sigalotti Ap.J. **389**, 386-391 (1992).
- [62] F. de Felice and Y. Yunqiang, Class. Quantm Grav. **10**, 353-364 (1993).